JOURNAL OF GEOPHYSICAL RESEARCH, VOL. 116, XXXXXX, doi:10.1029/2011JB008379, 2011

The timing of strike-slip shear along the Ranong and Khlong Marui faults, Thailand

Ian Watkinson,[1] Chris Elders,[1] Geoff Batt,[2] Fred Jourdan,[3] Robert Hall,[1] and Neal J. McNaughton[4]

Received 1 April 2011; accepted 10 June 2011; published XX Month 2011.

[1] The timing of shear along many important strike-slip faults in Southeast Asia, such as the Ailao Shan-Red River, Mae Ping and Three Pagodas faults, is poorly understood. We present $^{40}Ar/^{39}Ar$, U-Pb SHRIMP and microstructural data from the Ranong and Khlong Marui faults of Thailand to show that they experienced a major period of ductile dextral shear during the middle Eocene (48–40 Ma, centered on 44 Ma) which followed two phases of dextral shear along the Ranong Fault, before the Late Cretaceous (>81 Ma) and between the late Paleocene and early Eocene (59–49 Ma). Many of the sheared rocks were part of a pre-kinematic crystalline basement complex, which partially melted and was intruded by Late Cretaceous (81–71 Ma) and early Eocene (48 Ma) tin-bearing granites. Middle Eocene dextral shear at temperatures of ~300–500°C formed extensive mylonite belts through these rocks and was synchronous with granitoid vein emplacement. Dextral shear along the Ranong and Khlong Marui faults occurred at the same time as sinistral shear along the Mae Ping and Three Pagodas faults of northern Thailand, a result of India-Burma coupling in advance of India-Asia collision. In the late Eocene (<37 Ma) the Ranong and Khlong Marui faults were reactivated as curved sinistral branches of the Mae Ping and Three Pagodas faults, which were accommodating lateral extrusion during India-Asia collision and Himalayan orogenesis.

Citation: Watkinson, I., C. Elders, G. Batt, F. Jourdan, R. Hall, and N. J. McNaughton (2011), The timing of strike-slip shear along the Ranong and Khlong Marui faults, Thailand, *J. Geophys. Res.*, *116*, XXXXXX, doi:10.1029/2011JB008379.

1. Introduction

[2] Strike-slip faults are prominent features in Southeast Asia (Figure 1). Their development has been attributed to lateral extrusion driven by India-Asia collision (e.g., the Ailao Shan-Red River Fault [*Leloup et al.*, 1995]), partitioning of oblique subduction in the over-riding plate (e.g., the Sumatran Fault [*Fitch*, 1972]), and oblique collision or subduction transform edge propagation faulting (e.g., the Palu-Koro Fault [*Katili*, 1978; *Govers and Wortel*, 2005]), among other mechanisms [e.g., *Bertrand and Rangin*, 2003; *Morley*, 2004]. Thermochronological techniques such as $^{40}Ar/^{39}Ar$ dating constrain the history of complex structural systems, and have been applied to many such shear zones in Southeast Asia [e.g., *Lacassin et al.*, 1997; *Imtihanah*, 2000; *Wang et al.*, 2000]. It is becoming clear that individual structures can rarely be adequately explained by simple tectonic models, particularly those based on lateral extrusion of crustal blocks away from the Himalayan Orogeny [e.g., *Tapponnier et al.*, 1986].

[3] The Ranong Fault (RF) and Khlong Marui Fault (KMF) of the Thai peninsula have been considered conjugate structures to major NW trending faults in Northern Thailand and China (Figure 1), in a system entirely driven by far field intraplate forces caused by Indian indentation [*Tapponnier et al.*, 1982]. Numerous thermochronological studies of Southeast Asia's major strike-slip shear zones [e.g., *Schärer et al.*, 1994; *Leloup et al.*, 1995, 2001; *Lacassin et al.*, 1997; *Zhang and Schärer*, 1999; *Gilley et al.*, 2003], have revealed evidence of Oligocene to Miocene shear, but debate continues about whether this is due to extrusion tectonics, whether the faults penetrate to the mantle, and how much strain is focused on discrete block-bounding dislocations [e.g., *Wang et al.*, 2000; *Morley*, 2004; *Searle*, 2006, 2007; *Anczkiewicz et al.*, 2007; *Leloup et al.*, 2007; *Yeh et al.*, 2008].

[4] Despite the geographic and structural significance of Thailand's major strike-slip faults, few studies have attempted to date the timing of slip along them. Only one study has directly investigated the age of faults in Northern Thailand using the $^{40}Ar/^{39}Ar$ technique [*Lacassin et al.*,

[1]SE Asia Research Group, Department of Earth Sciences, Royal Holloway, University of London, UK.
[2]Centre for Exploration Targeting, John de Laeter Centre for Mass Spectrometry, University of Western Australia, Perth, Western Australia, Australia.
[3]Western Australian Argon Isotope Facility, Department of Applied Geology and John de Laeter Centre for Mass Spectrometry, Curtin University, Perth, Western Australia, Australia.
[4]Department of Imaging and Applied Physics, John de Laeter Centre for Mass Spectrometry, Curtin University, Perth, Western Australia, Australia.

0148-0227/11/2011JB008379

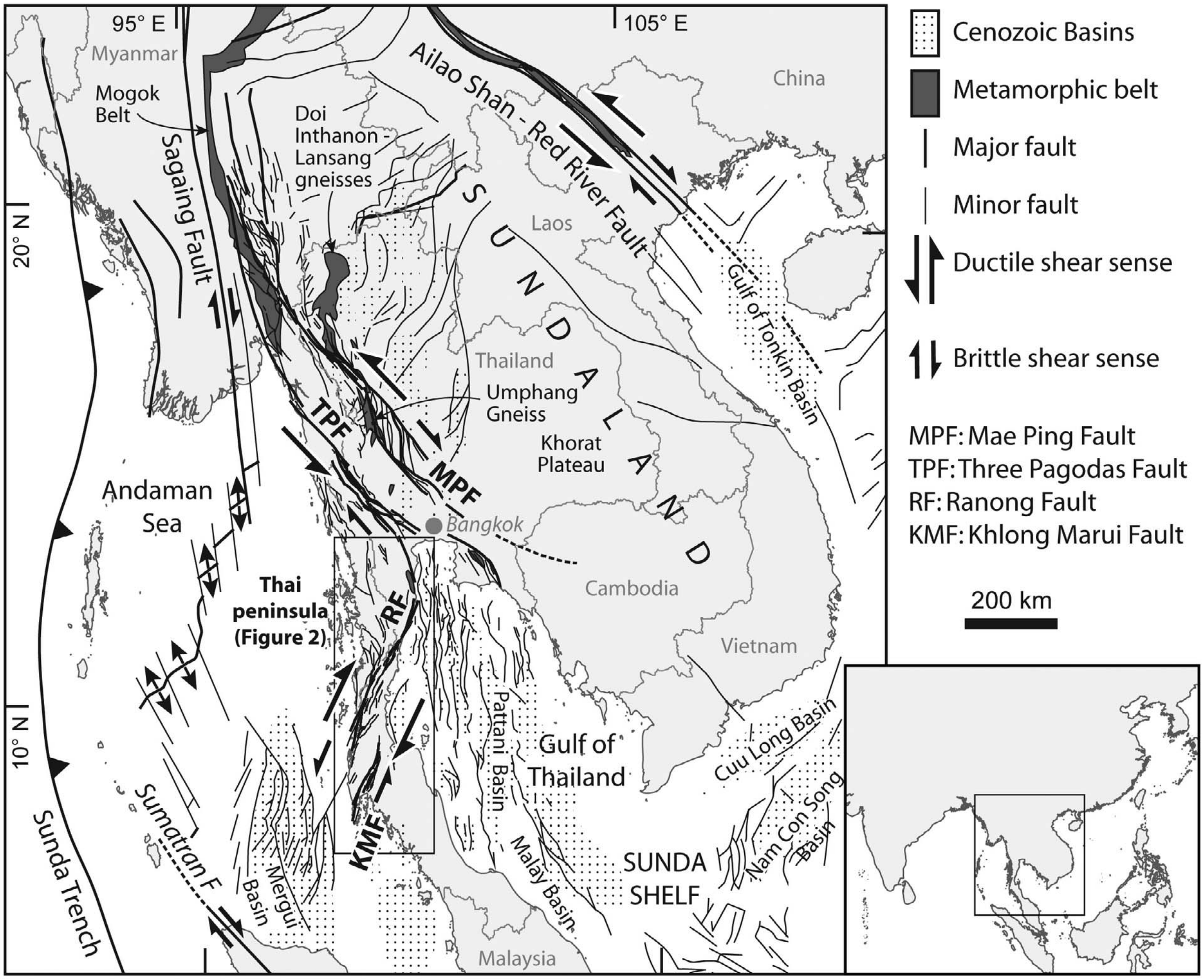

Figure 1. Regional tectonic map of Thailand and adjacent regions. Modified after *Leloup et al.* [1995], *Morley* [2002, 2004], and *Polachan* [1988]. A detailed map of the Thai peninsula (boxed) is given in Figure 2.

1997], and no previous study has been made of the peninsular faults. New information to constrain the nature and timing of deformation is necessary to explain the role they have played in the tectonic evolution of this complex region.

[5] We address this deficiency with new $^{40}Ar/^{39}Ar$ and U-Pb data to constrain the deformation history of these structures. The $^{40}Ar/^{39}Ar$ method was chosen for this study because it provides a spectrum of apparent ages, rather than a single 'total fusion' age, which aids the attribution of geological significance to ages and the identification of multiple thermal events. Additionally, direct comparison is possible with previous studies of Thailand that used the same technique [*Charusiri*, 1989; *Tulyatid*, 1991; *Lacassin et al.*, 1997]. Zircon U-Pb SHRIMP (Sensitive High Resolution Ion Microprobe) data are also presented to determine the emplacement age of deformed granitoids.

2. Tectonic Setting

[6] Western Thailand is part of the Sibumasu Terrane, a continental fragment that rifted from Gondwana during the Permian, and collided with the Indochina Terrane at the southeastern margin of Asia following northward subduction of Palaeo-Tethys [e.g., *Ridd*, 1971; *Metcalfe*, 1994, 1996, 2011; *Sone and Metcalfe*, 2008]. Collision was complete by the Late Triassic [*Metcalfe*, 2011; *Sevastjanova et al.*, 2011].

[7] Since the Late Triassic, Thailand has remained within the core of Sundaland: a heterogeneous region of weak and warm lithosphere that forms the southeastern promontory of Asia [*Hall*, 2002; *Hall and Morley*, 2004; *Hall et al.*, 2009]. Thailand experienced significant and complex deformation throughout Mesozoic to Cenozoic time. Andean-type magmatism in eastern Myanmar and Thailand [e.g., *Cobbing et al.*, 1986; *Putthapiban*, 1992; *Charusiri et al.*, 1993; *Barley et al.*, 2003] linked to Neo Tethys subduction may have heated and thickened Sibumasu during the Late Cretaceous to earliest Cenozoic [e.g., *Mitchell*, 1993; *Barley et al.*, 2003; *Searle et al.*, 2007].

[8] Late Cretaceous metamorphism and middle Eocene high temperature metamorphism of the Doi Inthanon – Lansang gneisses of western Thailand [*Dunning et al.*, 1995] correlate closely with events in the Mogok Belt of Myanmar (Figure 1), including Paleocene regional metamorphism

followed by high temperature metamorphism and crustal melting from the middle Eocene to the latest Oligocene [*Searle et al.*, 2007]. *Morley* [2004] proposed a period of transpression in western Thailand to explain features including long-lived and complex sinistral slip along the Mae Ping and Three Pagodas faults, Paleogene folds and thrusts, and Eocene uplift of the Khorat Plateau in east Thailand. *Searle and Morley* [2011] suggest that these features may be the result of India-West Burma coupling in advance of the main period of India-Asia collision.

[9] Much of mainland Southeast Asia, including western Thailand, is dominated by large strike-slip faults originating near the eastern Himalayan syntaxis. Their scale and clear topographic expression have led to models requiring hundreds of kilometers of focused strike-slip motion along each to accommodate eastward extrusion of fault-bounded blocks during the Cenozoic indentation of India into Eurasia [e.g., *Molnar and Tapponnier*, 1975; *Tapponnier and Molnar*, 1977; *Tapponnier et al.*, 1982, 1986; *Leloup et al.*, 1995; *Lacassin et al.*, 1997; *Gilley et al.*, 2003]. The faults include the Ailao Shan – Red River Fault (ASRR) in China and Vietnam, the Mae Ping Fault (or Wang Chao Fault) and the Three Pagodas Fault in Thailand. Sinistral motion was followed by a diachronous change to dextral motion during the Oligocene along the Mae Ping and Three Pagodas faults, and during the Pliocene to Quaternary along the ASRR [e.g., *Wang et al.*, 1998]. Northward younging slip sense reversal has been interpreted to result from northward migration of the Himalayan deformation front [*Lacassin et al.*, 1997].

[10] Recent studies of the faults (particularly the ASRR) have led to debate concerning the age, scale and significance of strike-slip motion [e.g., *Jolivet et al.*, 2001; *Anczkiewicz et al.*, 2007; *Searle*, 2007].

[11] A north-south belt of basins from the Gulf of Thailand to Laos developed from the Eocene to the Miocene [e.g., *Polachan et al.*, 1991; *Jardine*, 1997; *Morley*, 2002; *Hall and Morley*, 2004; *Morley and Westaway*, 2006]. In the north the basins are mostly associated with the Mae Ping and Three Pagodas faults and smaller strike-slip faults, and in the south, most are N-S trending extensional rifts [e.g., *Jardine*, 1997; *Uttamo et al.*, 2003]. Many basins are bounded by low angle normal faults, indicating basement fabric control [*Morley et al.*, 2011]. Low angle normal faults in northern Thailand exhumed the Doi Inthanon and Doi Suthep metamorphic core complexes between the late Oligocene and early Miocene [e.g., *Dunning et al.*, 1995; *Rhodes et al.*, 2000; *Barr et al.*, 2002].

[12] South and west of Thailand is the Sunda Trench, where Tethyan and Indian oceanic crust has been subducted during much of the Mesozoic and Cenozoic [*Hall*, 2002; *Hall et al.*, 2009]. Oblique Tethyan and Indian Ocean subduction, accretion of island arcs and continental fragments and subduction rollback have all influenced Thailand's tectonic evolution. The Andaman Sea, a Neogene back-arc basin inboard of the Sunda Trench [*Curray*, 2005], is linked, via the active dextral Sagaing Fault [e.g., *Bertrand and Rangin*, 2003; *Vigny et al.*, 2003], to the northward motion of West Burma after it became coupled to India [*Maung*, 1987]. Southeast of Thailand, the rest of Southeast Asia is a region of complex deformation, high rates of convergence [e.g., *Bock et al.*, 2003; *Simons et al.*, 2007], and a thin, warm and weak lithosphere [*Hall and Morley*, 2004], complexities that may have affected the region's response to distant events.

3. Geology and Shear Zones of the Thai Peninsula

3.1. Geology of the Thai Peninsula

[13] The Thai peninsula (Figures 1 and 2) is bounded by the Andaman Sea and the Gulf of Thailand. Major strike-slip faults are limited to the northern 700 km between Phuket and Bangkok. Much of the northern peninsula is covered by Carboniferous-Permian marine sediments of the Kaeng Krachan Group [*Ueno*, 2003], deposited during rifting of Sibumasu from Gondwana [*Ridd*, 2009]. They are composed of gray mudstone, siliceous shale, sandstone, characteristic diamictites and conglomeratic sequences 2–3 km thick. Permian Ratburi Group carbonates overlie this unit [*Bunopas*, 1981; *Fontaine et al.*, 1994], and sandstones and shales of the Jurassic to Cretaceous Thung Yai Group crop out on the east of the peninsula. The southern Thai peninsula, separated from the north by the KMF, has a markedly different stratigraphy. Cambrian to Lower Permian clastics, carbonates and low grade metasedimentary rocks crop out beneath a thin Kaeng Krachan Group, in which diamictites are rare. This has been interpreted by *Ridd* [2009] as evidence that the KMF originated as a late Paleozoic rift-bounding normal fault zone.

[14] A number of small Cenozoic basins on land, notably the Krabi Basin close to the KMF, contain upper Eocene to Oligocene sediments and are probably the same age as structurally similar basins offshore [*Ducrocq et al.*, 1995; *Chaimanee et al.*, 1997; *Intawong*, 2006].

[15] Exposures of medium to high grade metamorphic rocks undeformed by shear along the RF and KMF are limited to Precambrian to Carboniferous(?) age amphibolite facies orthogneisses and metasediments at the extreme northern end of the Ranong Fault, and east of the Khlong Marui Fault [e.g., *Pongsapitch et al.*, 1980; *Tulyatid*, 1991]. Intrusive igneous rocks are widespread. Granitoids of the Cretaceous-Eocene Western Granite Province occur along the northern peninsula, and Late Triassic-Early Jurassic Main Range Province granites crop out in the south [e.g., *Cobbing et al.*, 1986; *Charusiri*, 1989; *Putthapiban and Schwartz*, 1994].

3.2. The Ranong and Khlong Marui Faults

[16] The Ranong and Khlong Marui faults are NNE trending strike-slip structures that cut the Thai peninsula and

Figure 2. Overview map of the Thai peninsula, showing the Khlong Marui and Ranong faults. See Figure 1 for location. Boxes show details of individual ductile fault cores, sample locations, Ar-Ar plateaux (samples ending in B, M and H) and U-Pb emplacement ages (samples ending in Z). Base geology modified after *Dheeradilok et al.* [1985], *Hintong et al.* [1985], *Mahawat et al.* [1985], *Mantajit et al.* [1985], *Nakornsri et al.* [1985], *Silpalit et al.* [1985], and *Geological Survey of Japan* [1997].

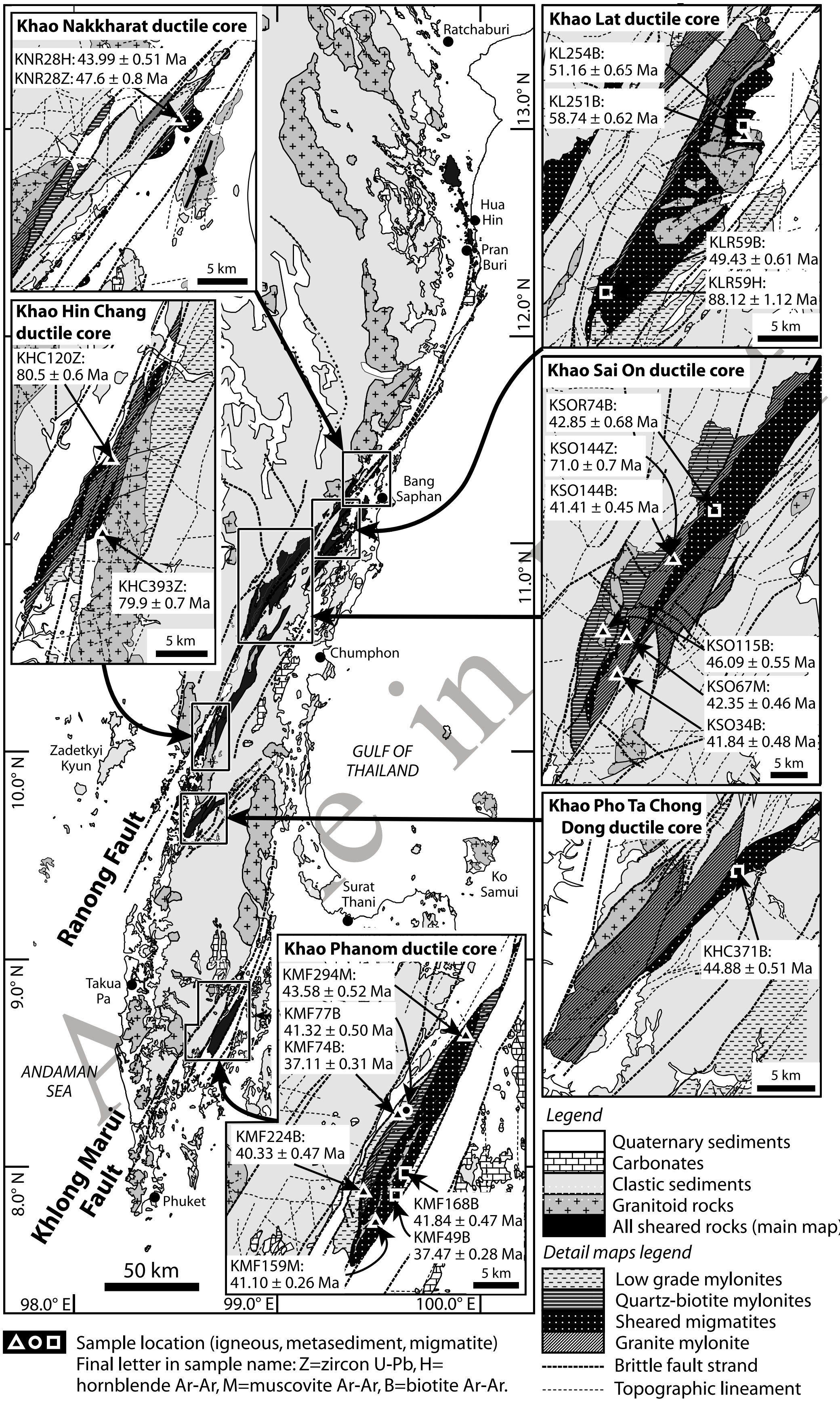
Khao Nakkharat ductile core
KNR28H: 43.99 ± 0.51 Ma
KNR28Z: 47.6 ± 0.8 Ma
5 km
Khao Hin Chang ductile core
KHC120Z: 80.5 ± 0.6 Ma
KHC393Z: 79.9 ± 0.7 Ma
5 km
Khao Lat ductile core
KL254B: 51.16 ± 0.65 Ma
KL251B: 58.74 ± 0.62 Ma
KLR59B: 49.43 ± 0.61 Ma
KLR59H: 88.12 ± 1.12 Ma
5 km
Khao Sai On ductile core
KSOR74B: 42.85 ± 0.68 Ma
KSO144Z: 71.0 ± 0.7 Ma
KSO144B: 41.41 ± 0.45 Ma
KSO115B: 46.09 ± 0.55 Ma
KSO67M: 42.35 ± 0.46 Ma
KSO34B: 41.84 ± 0.48 Ma
5 km
Khao Pho Ta Chong Dong ductile core
KHC371B: 44.88 ± 0.51 Ma
5 km
Khao Phanom ductile core
KMF294M: 43.58 ± 0.52 Ma
KMF77B 41.32 ± 0.50 Ma
KMF74B: 37.11 ± 0.31 Ma
KMF224B: 40.33 ± 0.47 Ma
KMF168B 41.84 ± 0.47 Ma
KMF49B 37.47 ± 0.28 Ma
KMF159M: 41.10 ± 0.26 Ma
5 km
Ratchaburi
Hua Hin
Pran Buri
Bang Saphan
Chumphon
Zadetkyi Kyun
GULF OF THAILAND
Surat Thani
Ko Samui
Takua Pa
ANDAMAN SEA
Phuket
Ranong Fault
Khlong Marui Fault
50 km
13.0° N
12.0° N
11.0° N
10.0° N
9.0° N
8.0° N
98.0° E
99.0° E
100.0° E
Legend
Quaternary sediments
Carbonates
Clastic sediments
Granitoid rocks
All sheared rocks (main map)
Detail maps legend
Low grade mylonites
Quartz-biotite mylonites
Sheared migmatites
Granite mylonite
Brittle fault strand
Topographic lineament
Sample location (igneous, metasediment, migmatite)
Final letter in sample name: Z=zircon U-Pb, H= hornblende Ar-Ar, M=muscovite Ar-Ar, B=biotite Ar-Ar.

Figure 2

deform all exposed lithologies (Figure 2). The faults have been described by *Watkinson et al.* [2008] and *Watkinson* [2009]. The two fault zones have similar topographic and geologic expression. Kilometer-scale slivers of strongly sheared mid-crustal rocks, including schists, migmatites, ortho- and paragneisses, crop out within, and are typically bounded by curvilinear brittle faults. Exposed slivers of ductile fault rocks bounded by brittle faults and surrounded by non-metamorphic rocks are termed 'ductile fault cores' here for simplicity. At least five ductile fault cores crop out along the RF, and a single one crops out within the KMF (Figure 2). An additional N-S trending belt of dextral mylonite is exposed near Pran Buri at the extreme northern end of the RF [e.g., *Charusiri*, 1989; *Tulyatid*, 1991; *Watkinson*, 2009]. Ductile fault cores are named after the mountain (*Khao*) on which they are centered. Details of ductile fault rocks from which the dated samples were collected are given below.

3.2.1. Sheared Migmatites

[17] Migmatite belts exposed along the RF and KMF are part of a pre-kinematic Paleozoic-Mesozoic regional metamorphic basement complex that was sheared and locally exhumed by movement along the faults. Biotite-rich stromatic (layered) migmatites are most common. Granitic leucosomes form fine intrafolial sheets, lenses, pods and larger veins (Figure 3a). Post-anatectic mylonitisation is ubiquitous and locally intense. Biotite and sillimanite define a schistose foliation that is locally deflected into oblique shear planes. All kinematic indicators indicate dextral shear. Stretched pebbles of quartz and granite (Figure 3b) indicate that the protolith may be glacio-marine [*Stauffer and Mantajit*, 1981] pebbly mudstones of the Kaeng Krachan Group, which crop out extensively outside the shear zones along the Thai peninsula. Locally quartz-biotite mylonites similar to the migmatite mesosome lack sillimanite and melt veins, and may be lower metamorphic grade equivalents of the stromatic migmatites. Boudinage of quartz layers within the mylonitic foliation is widespread (Figure 3c).

[18] Sheared gneissic nebulitic (diffuse) migmatites are limited to the central part of the RF, locally showing almost complete anatexis (Figure 3d). Diffuse hornblende melanosomes surround leucocratic areas. Hornblende and garnet form nuclei for asymmetric biotite pressure shadows. Post-anatectic mylonitic fabrics are more variably oriented than elsewhere in the fault zones, but kinematic indicators such as rolled porphyroclasts, stair-stepping and sigma-type objects, asymmetric boudinage and shear bands show dextral shear parallel to the RF.

3.2.2. Mylonitic Granite

[19] Kilometer-scale granitoid bodies that have experienced significant solid state deformation are closely associated with the migmatite belts. Rounded feldspar porphyroclasts have σ-type mantles of bulging dynamically recrystallized feldspar (Figure 3e). Biotite partly defines the mylonitic foliation and lineation, and is often drawn into shear bands and mica fish. Bulging recrystallization of quartz and sometimes feldspar occurs along shear planes. Most of the granites are part of the Cretaceous-Eocene Western Granitoid Province [e.g., *Cobbing et al.*, 1986; *Charusiri*, 1989; *Putthapiban and Schwartz*, 1994], and their mylonitic textures show that they were sheared after crystallization.

[20] Gneissic banding, schistosity and mylonitic foliations in most sheared rocks dip steeply, and a persistent mylonitic lineation plunges gently. These fabrics are sub-parallel to the ductile fault core margins and to the main brittle faults. Kinematic indicators, such as rolled porphyroclasts, shear bands, sheath folds, quarter folds, S-C′ fabrics (Figure 3f), mineral fish, oblique foliations in quartz, antithetic fractures in rigid grains, asymmetric fold vergence and asymmetric boudins, consistently indicate a dextral shear sense in all the mylonites.

[21] Recrystallization fabrics in mylonites can be used as a crude temperature gauge, assuming normal strain rates [*Passchier and Trouw*, 2005]. Mylonites from the RF and KMF exhibit syn-kinematic subgrain rotation (T~400°C) and localized grain boundary migration of quartz (T > 500°C), and bulging recrystallization of feldspar (T ~400–600°C) (Figure 3g). More rarely, bulging recrystallization of garnet, quartz 'chessboard' subgrains, subgrain rotation in feldspars and amphibole fish indicate temperatures greater than 600–700°C.

[22] Brittle faults bound the ductile fault cores. They are composed of fault breccias of mylonites and shallow level rocks, discrete moderate to steeply dipping fault planes and wide damage zones. Kinematic indicators in the brittle faults include sinistral and dextral strike-slip, oblique-slip and pure dip-slip senses. The dip-slip component, together with the geometry of the bounding faults indicates that they were involved in exhuming the older mylonites. Brittle faults also occur in non-mylonitic country rocks. Some of these faults may have formed during the younger brittle faulting, others may be upper crustal contemporaries of the exhumed dextral shear zones that have remained at shallow crustal levels.

4. Analytical Procedure

4.1. Sample Preparation

[23] Samples were collected during 2006–2007, mostly from river-polished outcrops. Twelve samples from the RF, and seven from the KMF were selected for analysis. Samples were chosen on the basis of their freshness and structural context. One to three kilograms of each sample were comminuted in a jaw crusher, and sieved using 63 μm, 100 μm, 250 μm, 0.5 mm and 2 mm meshes. Migmatite samples were first split into leucosome and mesosome parts using a diamond saw. Mineral grains were separated using heavy liquids (sodium polytungstate solution and di-iodomethane) and a Frantz magnetic separator, and hand picked. Nine mica, two amphibole and four zircon separates from the RF, and four mica separates from the KMF were selected for $^{40}Ar/^{39}Ar$ and U-Pb SHRIMP dating at Curtin University of Technology (Australia). Three additional mica separates from the KMF were selected for $^{40}Ar/^{39}Ar$ dating at the Noble Gas Laboratory, Institute of Mineralogy and Geochemistry, Université de Lausanne (Switzerland).

4.2. U-Pb Procedure

[24] Zircon grains were cast in an epoxy mount with chips of the BR266 reference standard (559 Ma; 903 ppm U) and the OGC standard for checking the $^{207}Pb/^{206}Pb$ age (3467 ± 3 Ma). After polishing to expose zircon grains in section, the SHRIMP mount (10–27) was gold coated and imaged on a Jeol 6400 scanning electron microscope to provide

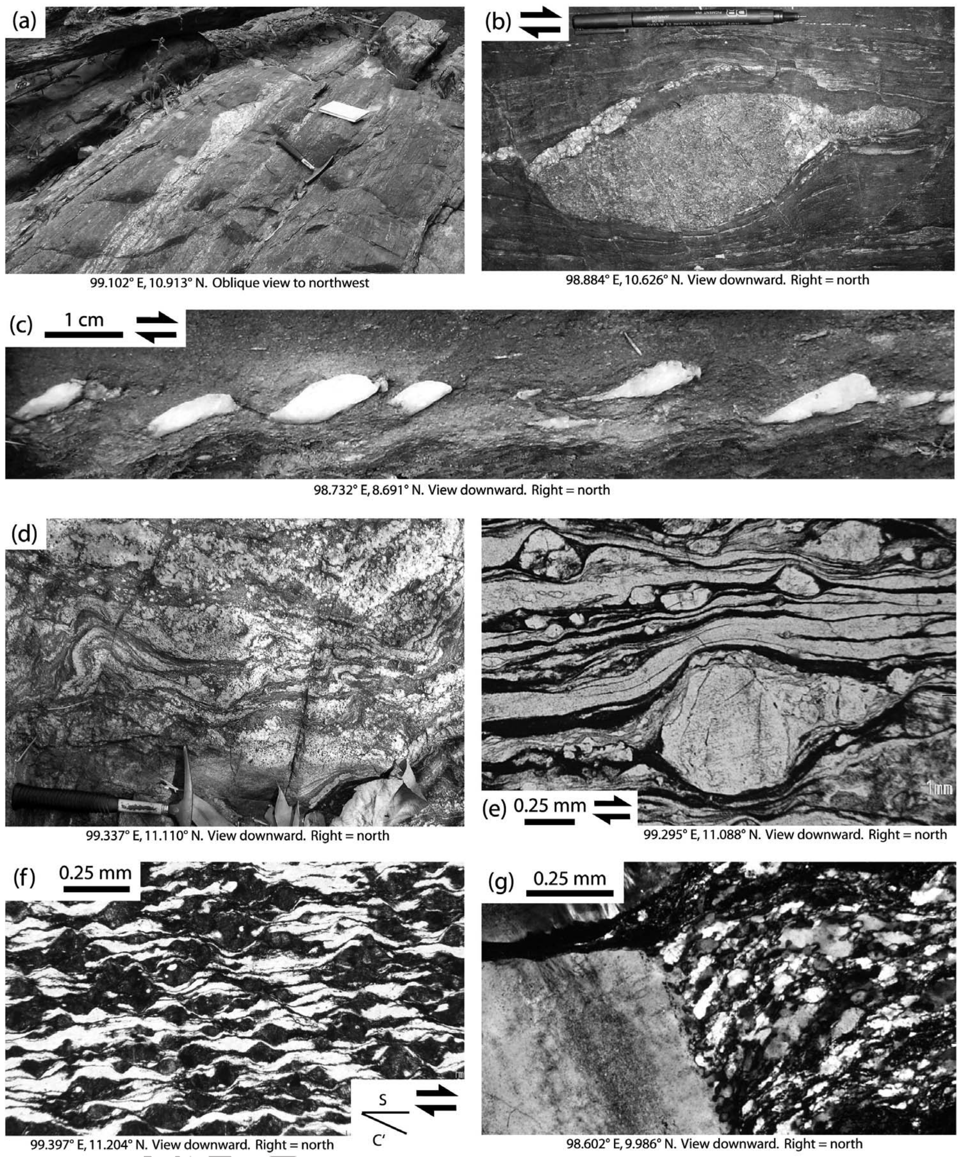

Figure 3. Characteristics of the ductile fault rocks. (a) Mylonitic stromatic migmatite, Khlong Sa Ang, northern Khao Sai On ductile core. (b) Sheared granite clast in quartz-biotite mylonites, Ban Nam Khao, southern Khao Sai On ductile core. (c) Asymmetric quartz boudin train in quartz-biotite mylonites, Khlong Song Phraek, central Khao Phanom ductile core. (d) Weakly sheared nebulitic migmatites, Huai Nong Chan Wong, northern Khao Lat ductile core. (e) Typical mylonitic granite texture, plane polarized light. Huai Tanao, central Khao Lat ductile core. (f) S-C′ fabric in mylonitic granite. Feldspar is badly weathered and appears dark in thin section. Plane polarized light. Khlong Yang Khwang, southern Khao Nakkharat ductile core. (g) Dynamic recrystallization of feldspar adjacent to a feldspar porphyroclast in a mylonitic granite, crossed polars. Khao Hin Chang, southern Khao Hin Chang ductile core.

cathodoluminescence images of the internal growth structure of the zircons (Figure 4), to aid selection of areas for analysis.

[25] Analyses were undertaken over two 24 h sessions with a near circular 25 μm diameter "spot" produced by a ~2 nA primary ion beam of O_2^-. Analytical procedures generally follow *Compston et al.* [1984] and *Smith et al.* [1998] and include rastering the ion beam over the analysis area to remove the gold coat and surface common Pb. The 207-correction for common Pb is utilized for analyses younger than 700 Ma, and the 204-correction for older analyses [*Compston et al.*, 1984]. Data were reduced using the SQUID software of *Ludwig* [2001]. Analytical data are shown in Table 1, sample locations and emplacement ages are marked on Figure 2 (samples ending in Z).

4.3. The ^{40}Ar/^{39}Ar Procedure

[26] Hornblende separates dated at the Western Australian Argon Isotope Facility at Curtin University of Technology were leached in diluted HF for one minute, and both hornblende and mica grains were thoroughly rinsed with distilled water in an ultrasonic cleaner. Samples were loaded into

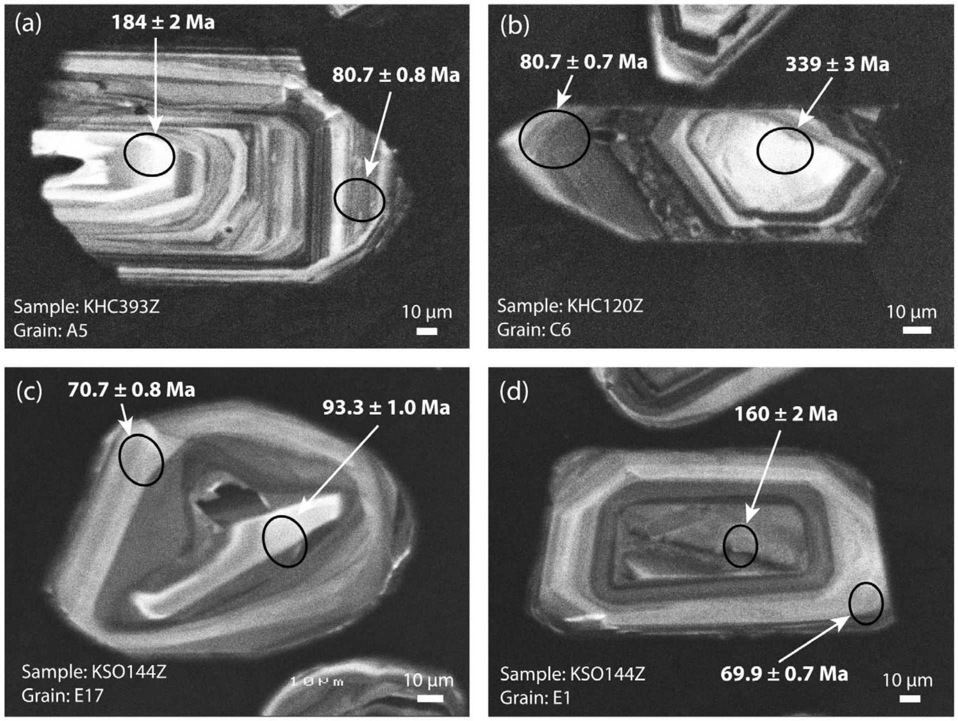

Figure 4. Cathodoluminescence images of dated zircons from the Ranong Fault, showing SHRIMP pits (circled) and ages. See Table 1 for details. (a) Sample KHC393Z, weakly foliated pre-kinematic granite, east of Khao Hin Chang ductile core. (b) Sample KHC120Z, mylonitic granite, central Khao Hin Chang ductile core. (c) Sample KSO144Z, mylonitic granite, central Khao Sai On ductile core. (d) Sample KSO144Z, mylonitic granite, central Khao Sai On ductile core.

sixteen large wells of one 1.9 cm diameter and 0.3 cm depth aluminum disc. These wells were bracketed by small wells that included Fish Canyon sanidine (FCs) as a neutron fluence monitor, for which an age of 28.03 ± 0.08 Ma was adopted [*Jourdan and Renne*, 2007]. The discs were Cd-shielded to minimize undesirable nuclear interference reactions, and irradiated for 25 h in the Hamilton McMaster University nuclear reactor, Canada, in position 5C. The mean J-values computed from standard grains within the small pits range from 0.0003500 ± 0.000002 (±0.57% uncertainty) to 0.0003579 ± 0.0000018 (±0.5% uncertainty) determined as the average and standard deviation of J-values of the small wells for each irradiation disc. Mass discrimination was monitored using an automated air pipette and provided a mean value of 1.005089 ± 0.002751 per dalton (atomic mass unit). The correction factors for interfering isotopes were $(^{39}Ar/^{37}Ar)_{Ca} = 7.30 \times 10^{-4}$ (±11%), $(^{36}Ar/^{37}Ar)_{Ca} = 2.82 \times 10^{-4}$ (±1%) and $(^{40}Ar/^{39}Ar)_K = 6.76 \times 10^{-4}$ (±32%).

[27] The mica samples were step-heated using a 110 W Spectron Laser System, with a continuous Nd-YAG (IR; 1064 nm) laser rastered across either single large grains or multigrain aliquots wrapped in zero-blank niobium foil, over a time period of approximately one minute to ensure a homogenously distributed temperature. The 20 mg hornblende samples were step-heated in a double vacuum high frequency Pond Engineering furnace. The gas was purified in a stainless steel extraction line using three SAES AP10 getters and a liquid nitrogen condensation trap. Argon isotopes were measured in static mode using a MAP 215–50 mass spectrometer (resolution of ~600; sensitivity of 2×10^{-14} mol/V) with a Balzers SEV 217 electron multiplier using 9 to 10 cycles of peak-hopping. Data acquisition was performed with the Argus program written by M.O. McWilliams and run under a LabView environment. The raw data were processed using ArArCALC software [*Koppers*, 2002] and the ages were calculated using decay constants recommended by *Steiger and Jäger* [1977]. Laser blanks were monitored every 3 to 4 steps and typical ^{40}Ar blanks range from 1×10^{-16} to 2×10^{-16} mol. Furnace blanks were monitored every 3 samples and range from 3 to 10 times the laser blanks.

[28] Mineral separates dated at the Université de Lausanne were sealed in quartz vials then wrapped in cadmium and irradiated for 20 MWH in the CLICIT facility at the Oregon State University TRIGA reactor. Monitoring of the neutron flux was done using Fish Canyon Tuff sanidine, assuming an age of 28.03 ± 0.08 Ma [*Jourdan and Renne*, 2007] and isotopic production ratios were determined from irradiated CaF_2 and KCl salts. For this irradiation, the following production values were measured: $^{(36/37)}Ca = 0.0002609 \pm 0.00000508$; $^{(39/37)}Ca = 0.00068 \pm 0.000011$; and $^{(38/39)}K = 0.0122 \pm 0.000028$. One to several grains of the samples and the sanidines were loaded into 3 mm wells in a custom stainless steel planchette, and mounted in a sample chamber with a double-pumped ZnS window. The sample chamber was attached to a fully automated extraction line evacuated to UHV conditions and the samples were incrementally degassed using a 20W CO_2 laser. The sample gas was expanded and purified by exposure to a cold finger

Table 1. Zircon U-Pb SHRIMP Data From Granitoids Along the RF[a]

Sample-Grain-Spot	U (ppm)	Th (ppm)	232Th/238U	% common 206Pb	207Pb/206Pb +/−1s	206Pb/238U +/−1s	Age +/−1s (Ma)
Sample KHC393Z, Unfoliated, Pre-Kinematic Biotite-Tourmaline Granite, 98.65649E, 10.01911N[b]							
KHC393Z-1-1	839	392	0.48	0.75	0.042 +/− 0.005	0.0127 +/− 0.0001	81.1 +/− 0.9
KHC393Z-2-1	530	440	0.86	0.75	0.047 +/− 0.009	0.0124 +/− 0.0002	79.6 +/− 1
KHC393Z-3-1	598	382	0.66	0.93	0.055 +/− 0.004	0.0124 +/− 0.0002	79.2 +/− 1
KHC393Z-4-1	802	387	0.5	1.29	0.044 +/− 0.006	0.0124 +/− 0.0001	79.3 +/− 0.9
KHC393Z-5-1	1673	491	0.3	0.15	0.048 +/− 0.002	0.0126 +/− 0.0001	80.7 +/− 0.8
KHC393Z-5-2[c]	324	176	0.56	0.63	0.042 +/− 0.005	0.029 +/− 0.0004	184 +/− 2
KHC393Z-6-1	2173	588	0.28	0.29	0.045 +/− 0.002	0.0126 +/− 0.0001	80.7 +/− 0.7
KHC393Z-6-2[c]	946	390	0.43	2.75	0.048 +/− 0.009	0.0127 +/− 0.0002	81.7 +/− 1
KHC393Z-7-1[d]	165	234	1.47	3.42	0.035 +/− 0.02	0.0117 +/− 0.0002	74.8 +/− 1.6
KHC393Z-8-1	1067	418	0.4	0.45	0.048 +/− 0.002	0.0127 +/− 0.0001	81.2 +/− 0.9
KHC393Z-9-1	2940	728	0.26	0.04	0.047 +/− 0.001	0.0131 +/− 0.0001	84.1 +/− 0.7
KHC393Z-10-1	754	472	0.65	1.23	0.057 +/− 0.002	0.0122 +/− 0.0001	78.3 +/− 0.9
KHC393Z-11-1	1739	575	0.34	0.22	0.051 +/− 0.001	0.0125 +/− 0.0001	79.9 +/− 0.8
KHC393Z-12-1	2520	823	0.34	0.18	0.045 +/− 0.002	0.0124 +/− 0.0001	79.3 +/− 0.7
KHC393Z-13-1	1593	698	0.45	0.62	0.046 +/− 0.003	0.0123 +/− 0.0001	78.9 +/− 0.8
Sample KHC120Z, Foliated Biotite-Hornblende Granite, 98.66458E, 10.08686N[e]							
KHC120Z-1-1	3181	45	0.01	0.29	0.048 +/− 0.002	0.0126 +/− 0.0001	80.4 +/− 0.7
KHC120Z-2-1	3148	50	0.02	0.11	0.047 +/− 0.002	0.0127 +/− 0.0001	81.6 +/− 0.7
KHC120Z-3-1	1831	115	0.06	0.94	0.055 +/− 0.001	0.0151 +/− 0.0001	96.7 +/− 0.9
KHC120Z-4-1	3710	65	0.02	0.16	0.048 +/− 0.001	0.0125 +/− 0.0001	79.8 +/− 0.7
KHC120Z-5-1	3992	67	0.02	0.18	0.049 +/− 0.001	0.0125 +/− 0.0001	79.9 +/− 0.7
KHC120Z-6-1	3321	57	0.02	0.44	0.05 +/− 0.001	0.0126 +/− 0.0001	80.7 +/− 0.7
KHC120Z-1-2[c,f]	360	304	0.87	0.11	0.1355 +/− 0.002	0.0627 +/− 0.0012	762 +/− 7
KHC120Z-2-2[c,f]	481	1777	3.82	0.29	0.0128 +/− 0.0002	0.0504 +/− 0.0018	82 +/− 1
KHC120Z-3-2[c,f]	76	124	1.68	0.26	0.136 +/− 0.0021	0.0637 +/− 0.0025	731 +/− 82
KHC120Z-5-2[c,f]	1925	94	0.05	0.19	0.0763 +/− 0.0007	0.0576 +/− 0.0004	474 +/− 4
KHC120Z-6-2[c,f]	601	187	0.32	0.47	0.054 +/− 0.0005	0.056 +/− 0.0009	339 +/− 3
KHC120Z-7-1[c,f]	685	673	1.01	0.35	0.013 +/− 0.0001	0.0474 +/− 0.0018	83.2 +/− 0.9
KHC120Z-7-2[c,f]	512	168	0.34	0.34	0.0124 +/− 0.0001	0.0408 +/− 0.0036	79.5 +/− 0.9
KHC120Z-8-1[c,f]	96	138	1.48	0.15	0.0816 +/− 0.0012	0.061 +/− 0.0021	506 +/− 7
KHC120Z-9-1[c,d,f]	792	281	0.37	1.33	0.4439 +/− 0.0039	0.1614 +/− 0.0008	2471 +/− 8
KHC120Z-9-2[c,d,f]	917	373	0.42	1.84	0.4321 +/− 0.0038	0.1604 +/− 0.0004	2549 +/− 5
KHC120Z-10-1[c,f]	678	309	0.47	0.47	0.0115 +/− 0.0001	0.0511 +/− 0.0032	73.8 +/− 0.8
KHC120Z-11-1[c,f]	372	31	0.09	−0.44	0.0222 +/− 0.0003	0.0522 +/− 0.0036	142 +/− 2
KHC120Z-12-1[c,f]	1465	1362	0.96	0.15	0.0126 +/− 0.0001	0.0437 +/− 0.003	80.7 +/− 0.8
KHC120Z-12-2[c,f]	779	653	0.87	0.41	0.012 +/− 0.0001	0.0532 +/− 0.002	77.1 +/− 0.8
KHC120Z-13-1[f]	1000	1604	1.66	0.17	0.0125 +/− 0.0001	0.0504 +/− 0.0012	79.8 +/− 0.8
KHC120Z-14-1[f]	759	409	0.56	0.27	0.0127 +/− 0.0001	0.0563 +/− 0.0051	81.1 +/− 0.9
Sample KSO144Z, Foliated Biotite Granite, 98.98412 E, 10.79308 N[g]							
KSO144Z-1-1[f]	903	93	0.11	0.05	0.0109 +/− 0.0001	0.0381 +/− 0.004	69.9 +/− 0.7
KSO144Z-1-2[c,f]	1982	58	0.03	0.06	0.0251 +/− 0.0002	0.0505 +/− 0.0011	160 +/− 2
KSO144Z-2-1[c,d,f]	680	167	0.25	1.81	0.0917 +/− 0.0009	0.0724 +/− 0.0021	566 +/− 5
KSO144Z-3-1[f]	990	60	0.06	−0.14	0.0166 +/− 0.0002	0.0455 +/− 0.0023	106.1 +/− 1.2
KSO144Z-3-2[c,d,f]	1211	81	0.07	2.01	0.0798 +/− 0.0007	0.0729 +/− 0.0006	495 +/− 5
KSO144Z-4-1[f]	1342	83	0.06	−0.01	0.0109 +/− 0.0001	0.045 +/− 0.0015	70.1 +/− 0.7
KSO144Z-5-1[f]	763	99	0.13	0.46	0.0112 +/− 0.0001	0.0492 +/− 0.0017	71.9 +/− 0.8
KSO144Z-6-1[f]	830	103	0.13	0.16	0.0112 +/− 0.0001	0.045 +/− 0.0019	71.8 +/− 0.8
KSO144Z-7-1[f]	867	99	0.12	0.43	0.0111 +/− 0.0001	0.047 +/− 0.0015	70.9 +/− 0.8
KSO144Z-7-2[c,d,f]	430	223	0.54	2.43	0.2083 +/− 0.0019	0.1 +/− 0.0007	1623 +/− 13
KSO144Z-8-1[f]	949	113	0.12	0.28	0.0111 +/− 0.0001	0.0462 +/− 0.003	71.3 +/− 0.8
KSO144Z-9-1[f]	784	98	0.13	0.4	0.0115 +/− 0.0001	0.0396 +/− 0.0039	73.6 +/− 0.8
KSO144Z-10-1[f]	694	96	0.14	0.32	0.0106 +/− 0.0001	0.0483 +/− 0.0031	67.9 +/− 0.8
KSO144Z-10-2[c,f]	135	61	0.47	0.28	0.0338 +/− 0.001	0.0372 +/− 0.006	214 +/− 6
KSO144Z-11-1[f]	822	103	0.13	0.23	0.0112 +/− 0.0001	0.0533 +/− 0.0015	71.7 +/− 0.8
KSO144Z-12-1[f]	1138	140	0.13	0.04	0.023 +/− 0.0002	0.0494 +/− 0.0032	147 +/− 2
KSO144Z-13-1[f]	1475	158	0.11	−0.13	0.0226 +/− 0.0009	0.0476 +/− 0.0013	144 +/− 6
KSO144Z-14-1[f]	2032	267	0.14	0.06	0.0266 +/− 0.0002	0.0482 +/− 0.0009	169 +/− 2
KSO144Z-15-1[f]	1519	263	0.18	−0.19	0.019 +/− 0.0002	0.0452 +/− 0.0013	121.5 +/− 1.1
KSO144Z-16-1[f]	2440	151	0.06	0.12	0.0201 +/− 0.0004	0.0489 +/− 0.0007	128.5 +/− 2.7
KSO144Z-17-1[f]	828	125	0.16	0.16	0.011 +/− 0.0001	0.0526 +/− 0.0028	70.7 +/− 0.8
KSO144Z-17-2[c,f]	1004	24	0.02	0.54	0.0146 +/− 0.0002	0.0542 +/− 0.0014	93.3 +/− 1
KSO144Z-18-1[f]	2054	144	0.07	0.11	0.0187 +/− 0.0002	0.0496 +/− 0.0007	119.4 +/− 1.1
KSO144Z-19-1[f]	1584	95	0.06	0.06	0.0113 +/− 0.0001	0.0485 +/− 0.0013	72.5 +/− 0.7
KSO144Z-20-1[f]	710	89	0.13	0.15	0.0115 +/− 0.0001	0.0477 +/− 0.0023	73.6 +/− 0.8
KSO144Z-21-1[f]	2469	294	0.12	0.02	0.0287 +/− 0.0003	0.0498 +/− 0.0011	182 +/− 2
Sample KNR28Z, Foliated Biotite-Hornblende Granite, 99.48517 E, 11.3557 N[h]							
KNR28Z-1-1	1473	563	0.4	0.31	0.047 +/− 0.004	0.0075 +/− 0.0001	48.3 +/− 0.5
KNR28Z-2-1	2110	995	0.49	0.37	0.049 +/− 0.003	0.0078 +/− 0.0001	49.9 +/− 0.5

Table 1. (continued)

Sample-Grain-Spot	U (ppm)	Th (ppm)	232Th/238U	% common 206Pb	207Pb/206Pb +/−1s	206Pb/238U +/−1s	Age +/−1s (Ma)
KNR28Z-3-1	1148	244	0.22	0.73	0.05 +/− 0.004	0.0068 +/− 0.0001	43.7 +/− 0.5
KNR28Z-4-1	1011	940	0.96	1.21	0.047 +/− 0.007	0.0069 +/− 0.0001	44.2 +/− 0.6
KNR28Z-5-1	1469	499	0.35	0.66	0.054 +/− 0.002	0.0076 +/− 0.0001	48.6 +/− 0.5
KNR28Z-6-1	1153	691	0.62	0.61	0.052 +/− 0.004	0.0074 +/− 0.0001	47.7 +/− 0.6
KNR28Z-7-1	670	565	0.87	1.21	0.051 +/− 0.004	0.0075 +/− 0.0001	48 +/− 0.7
KNR28Z-8-1	919	307	0.35	0.52	0.047 +/− 0.003	0.0073 +/− 0.0001	46.9 +/− 0.6
KNR28Z-9-1	1369	615	0.46	0.77	0.055 +/− 0.002	0.0076 +/− 0.0001	48.6 +/− 0.5
KNR28Z-10-1	1771	838	0.49	0.75	0.058 +/− 0.004	0.0075 +/− 0.0001	48.2 +/− 0.5
KNR28Z-11-1	895	371	0.43	0.68	0.04 +/− 0.005	0.0073 +/− 0.0001	47.1 +/− 0.6
KNR28Z-12-1	1388	535	0.4	0.26	0.045 +/− 0.005	0.0076 +/− 0.0001	48.8 +/− 0.5
KNR28Z-13-1	1438	608	0.44	0.97	0.056 +/− 0.002	0.0073 +/− 0.0001	47 +/− 0.5
KNR28Z-14-1	923	314	0.35	0.87	0.064 +/− 0.002	0.0073 +/− 0.0001	47.2 +/− 0.6
KNR28Z-15-1	1189	459	0.4	0.55	0.049 +/− 0.003	0.0074 +/− 0.0001	47.5 +/− 0.6
KNR28Z-16-1	1237	461	0.39	−0.17	0.06 +/− 0.002	0.0076 +/− 0.0001	48.6 +/− 0.6
KNR28Z-2-2[f]	404	106	0.27	0.47	0.0072 +/− 0.0001	0.0503 +/− 0.0106	46.6 +/− 0.7
KNR28Z-3-2[f]	1480	416	0.29	0.1	0.0077 +/− 0.0001	0.0475 +/− 0.0023	49.3 +/− 0.5
KNR28Z-5-2[c,f]	356	104	0.3	0.23	0.0074 +/− 0.0001	0.0221 +/− 0.0109	47.3 +/− 0.7
KNR28Z-5-3[f]	736	286	0.4	−0.01	0.0074 +/− 0.0001	0.0332 +/− 0.0056	47.2 +/− 0.6
KNR28Z-7-2[f]	430	474	1.14	0.44	0.0075 +/− 0.0001	0.0484 +/− 0.0086	48 +/− 0.7
KNR28Z-7-3[c,f]	355	575	1.67	0.94	0.0072 +/− 0.0001	0.0411 +/− 0.0103	46.2 +/− 0.7
KNR28Z-11-2[c,f]	500	143	0.29	0.44	0.0072 +/− 0.0001	0.0574 +/− 0.0049	46.5 +/− 0.6
KNR28Z-17-1[f]	728	278	0.39	−0.18	0.0075 +/− 0.0001	0.0277 +/− 0.0061	48.3 +/− 0.6

[a]All Pb isotope ratios are corrected for common Pb: 204-correction for 207Pb/206Pb; and 207-correction for 206Pb/238U ratio and age, except for ages >700 Ma for which the 204-corrected Pb/U ratios are shown. Ages shown are 206Pb/238U ages except where >700 Ma, in which case 207Pb/206Pb ages are shown.
[b]Emplacement age: 79.9 +/− 0.7 Ma (2σ; n = 11, MSWD = 1.25).
[c]Analysis of zircon core; all others were from zircon rims.
[d]High common Pb correction: excluded from age discussion.
[e]Emplacement age: 80.5 +/− 0.6 Ma (2σ; n = 10, MSWD = 0.98).
[f]Reproducibility of the Pb/U for the standard zircon BR266 was 1.60% (2σ; n = 12); all others were +/−1.51% (2σ; n = 10).
[g]Emplacement age: 71.0 +/− 0.7 Ma (2σ; n = 8, MSWD = 1.05).
[h]Emplacement age: 47.6 +/− 0.8 Ma (2σ; n = 17, MSWD = 1.4).

maintainedat −132°C, and a SAES GP50 getter. The purified gas was then expanded into a Nu Instruments Noblesse mass spectrometer and isotopic ratios were measured in static mode. For this study argon isotopes were measured using a Faraday detector for m/e 40, and ion counting multipliers for m/e 39, 38, 37, and 36. Data were collected for a period of 300 s, and time zero intercepts were determined by linear regression of the data. Inter-calibration of the detectors was done using repeated air pipette measurements. Data were collected for a period of 300 s, and intercepts were determined by time zero regression of the data.

[29] Data and ages reported in Table 2 and Data Set S1 of the auxiliary material have been corrected for blanks, mass discrimination, radioactivity subsequent to irradiation, and interfering isotopic reactions.[1] Sample locations and plateau ages are marked on Figure 2 (samples ending B, H and M).

5. Results

[30] Tera-Wasserburg and age-frequency plots of SHRIMP U-Pb results are presented in Figure 5. In this study, the emphasis during zircon analysis is on rim ages. None of the deformation occurred under conditions hot enough to grow new zircon rims or significantly alter existing rims. Therefore the youngest rim ages are taken to record emplacement ages. Older cores represent inherited grains, and are not considered further here.

[31] Gas release spectra for $^{40}Ar/^{39}Ar$ analyses from samples from the KMF are presented in Figure 6, and spectra from RF samples are presented in Figures 7 and 8. Plateau, inverse isochron, and total fusion ages, MSWD and probability values are summarized in Table 2. Complete analytical data are presented in Data Set S1 of the auxiliary material. Inverse "isochron" and total fusion ages are not considered in this study because we demonstrate that there is systematic structure in the age spectra, invalidating the assumptions under which these methods have geological significance.

[32] Many of the dated mica samples exhibit well defined and consistent flat age spectra. This probably indicates, first, that radiogenic argon (^{40}Ar) is distributed evenly throughout the sample grains, and second, that there has been little thermal disturbance since crystallization, or since the $^{40}Ar/^{39}Ar$ system last rapidly closed. Our preferred interpretation is that the well expressed plateaux reflect individual episodes of rapid cooling. The similar plateau character and age resulting from analyses of both multigrain aliquots of fine (63–100 μm, e.g., KMF77B) mica grains, and coarse (0.5–1 mm, e.g., KSO34B) individual grains from comparable areas and structural domains rule out the alternative of gradual cooling, where such grain size differences might be expected to result in significant intrasample age gradients, and younger ages for finer material.

5.1. Khao Hin Chang Ductile Fault Core (Ranong Fault)

[33] A north-south trending, tourmaline bearing, coarse grained porphyritic biotite ± muscovite granite pluton east

[1]Auxiliary materials are available at ftp://ftp.agu.org/apend/jb/2011jb008379.

Table 2. Summary of $^{40}Ar/^{39}Ar$ Data and Ages From the Thai Peninsula

General Characteristics						Plateau Characteristics				Isochron Characteristics			
Sample	Location	Rock Type[a]	Min[b]	Lab[c]	Total Fusion Age (Ma, ±2σ)	Plateau Age (Ma, ±2σ)	Total ^{39}Ar Released (%)	MSWD	P	Isochron Age (Ma, ±2σ)	n	$^{40}Ar/^{36}Ar$ Intercept (±2σ)	MSWD
						Khlong Marui Fault							
KMF224B	98.69414 E, 8.59753 N	Gr myl	B	1	40.29 ± 0.47	40.33 ± 0.47	93.64	0.89	0.5	39.95 ± 0.0.6	10	330.97 ± 35	0.39
KMF168B	98.72895 E, 8.62111 N	Mig mes	B	1	41.48 ± 0.46	41.84 ± 0.47	95.31	1.7	0.1	41.60 ± 0.48	14	316.98 ± 16	1.15
KMF77B	98.73208 E, 8.6907 N	Qz-bt myl	B	1	41.40 ± 0.50	41.32 ± 0.50	99.49	1.18	0.3	41.27 ± 0.58	8	300.69 ± 42	1.36
KMF294M	98.79805 E, 8.7665 N	Mu-feld vein	M	1	43.60 ± 0.52	43.58 ± 0.52	100	1.07	0.4	42.98 ± 0.58	14	340.68 ± 28	1.47
KMF49B	98.72121 E, 8.60499 N	Mig mes	B	2	37.2 ± 0.2	37.47 ± 0.28	81.5	1.3	0.2				
KMF74B	98.72996 E,8.68966 N	Gr myl	B	2	38.1 ± 0.3	37.11 ± 0.31	67.9	1.5	0.1				
KMF159M	98.70016 E, 8.57776 N	Mu-feld vein	M	2	41.0 ± 0.3	41.10 ± 0.26	79.1	1.14	0.3				
						Ranong Fault							
KHC371B	98.69006 E, 9.74049 N	Mig mes	B	1	44.89 ± 0.51	44.88 ± 0.51	100	0.68	0.8	44.77 ± 0.51	12	308.74 ± 16	0.56
KSO34B	98.91445 E, 10.66079 N	Gr myl	B	1	41.83 ± 0.47	41.84 ± 0.48	99.45	1.3	0.2	41.81 ± 0.48	11	305.11 ± 15	1.13
KSO67M	98.91856 E, 10.70312 N	Mu-feld vein	M	1	42.36 ± 0.47	42.35 ± 0.46	99.87	1.1	0.4	42.36 ± 0.50	11	305.11 ± 15	1.15
KSOR74B	99.03561 E, 10.8447 N	Mig mes	B	1	42.84 ± 0.70	42.85 ± 0.68	100	0.44	1	42.97 ± 0.73	13	276.99 ± 75	0.7
KSO115B	98.89061 E, 10.70396 N	Bt granite	B	1	45.79 ± 0.53	46.09 ± 0.55	82.93	1.6	0.1	46.38 ± 0.59	14	242.61 ± 43	1.32
KSO144B	98.98412 E, 10.79308 N	Gr myl	B	1	41.52 ± 0.48	41.41 ± 0.45	86.38	0.43	0.9	41.37 ± 0.69	8	299.08 ± 45	0.51
KLR59B	99.22729 E, 10.98123 N	Mig undiff.	B	1	49.17 ± 0.61	49.43 ± 0.61	88.79	0.74	0.7	49.34 ± 0.73	16	301.09 ± 31	0.78
KLR59H	99.22729 E, 10.98123 N	Mig undiff.	H	1	87.60 ± 0.77	88.12 ± 1.12	77.57	2.3	0.1	88.52 ± 1.86	3	273.40 ± 82	4.06
KL251B	99.34213 E, 11.10707 N	Bt granite	B	1	58.61 ± 0.62	58.74 ± 0.62	98.17	1.3	0.2	58.59 ± 0.70	12	306.77 ± 25	1.27
KL254B	99.33714 E, 11.11018 E	Mig undiff.	B	1	50.90 ± 0.65	51.16 ± 0.65	87.03	0.5	0.7	51.52 ± 0.89	4	267.98 ± 46	0.03
KNR28H	99.48517 E, 11.3557 N	Gr myl	H	1	44.77 ± 0.56	43.99 ± 0.51	94.83	0.96		44.03 ± 0.68	7	292.12 ± 19	1.09

[a]Lithology: Gr myl, granite mylonite; Mig mes, migmatite mesosome; Mig leu, migmatite leucosome; Qz-bt myl, quartz-biotite mylonite; Mu-feld vein, muscovite-feldspar (+/− garnet) vein; Mig undiff, undifferentiated migmatite.
[b]Dated mineral: B, biotite; M, muscovite; H, hornblende.
[c]Laboratory: 1, Western Australian Argon Isotope Facility; 2, Université de Lausanne.

of Ranong town is truncated by a major ductile shear zone at Khao Hin Chang, near the southern end of the RF (Figures 2 and 9). The shear zone is at least 4 km wide and 33 km long, trends NNE, has steeply dipping foliations and gently plunging lineations, and bears consistently dextral kinematic indicators. It is largely composed of mylonitic granite, with smaller slivers of locally anatectic quartz-biotite mylonites densely intruded by pre-kinematic granitic veins. The undeformed Ranong granite grades, over a few hundred meters perpendicular to the shear zone trend, into proto-mylonites, mylonites and ultramylonites within the shear zone in the west. A kilometer-scale dextral sigmoidal deflection of the mylonitic foliation from the margin of the granite into the shear zone (Figure 9) also suggests that the Ranong granite is the protolith for the shear zone. The present-day contact between the granite and the shear zone is a brittle strike-slip fault zone with several kilometers of *sinistral* displacement.

[34] Zircon sample KHC393Z is from a weakly foliated porphyritic biotite granite at the very edge of the shear zone (Figure 2). Fifteen SHRIMP analyses on 13 zircon grains yielded ages around 80 Ma, mostly from grain rims (Figure 5). Omitting one analysis (#7–1) with unacceptably high common Pb correction, and an inherited core (spot A5–2, 184 ± 2 Ma), the remaining 13 analyses show scatter in excess of that expected for a single age population (i.e., MSWD = 3.7). Omitting the two oldest analyses (including the second core analysis #6–2), under the assumption they overlap with inherited ages, lowers the MSWD to an acceptable level for a single population at 79.9 ± 0.7 Ma (2σ; n = 11; MSWD = 1.25). This is taken to be the emplacement age of the rock.

[35] Zircon sample KHC120Z is from a strongly mylonitic biotite granite close to the western edge of the exposed shear zone (Figure 2). It is considered to be part of the same intrusion or suite of intrusions as the undeformed Ranong granite and its foliated margin (sample KHC393Z). Twenty-two SHRIMP analyses on 14 zircon grains show a considerable variation of ages from >2.4 Ga to ~80 Ma. About half the analyses are >90 Ma and come from zircon cores. Of the <90 Ma analyses, two groups are distinguished by Th/U. Five rim analyses have high U (3,000–4,000 ppm; Table 1) and distinctively low Th/U (0.01–0.02), whereas eight cores and rims have more variable U (500–1500 ppm) and higher Th/U (0.3–3.8). The age of the two groups is indistinguishable: 80.5 ± 0.8 Ma (2σ; n = 5; MSWD = 1.02) for the low-Th/U group, and 80.6 ± 0.9 Ma (2σ; n = 5; MSWD = 1.18) for the high-Th/U group, after omitting the two youngest (#10–1, #12–2) and oldest (#7–1) as statistical outliers. The combined result is 80.5 ± 0.6 Ma (2σ; n = 10; MSWD = 0.98), considered to be the age of emplacement. This is coincident with KHC393Z, supporting our hypothesis that the two samples belong to the same, pre-kinematic intrusion suite. Shear must therefore have occurred after the ~80 Ma emplacement of the Ranong granite.

[36] About 30 km south of Ranong town, a ~30 × 5 km belt of mylonitic rocks is exposed at Khao Pho Ta Chong Dong (Figure 2). It includes sheared granites, migmatites and quartz-biotite mylonites. Dextral kinematic indicators are abundant. Biotite from the mesosome of a sheared stromatic migmatite (KHC371B) yielded an $^{40}Ar/^{39}Ar$ plateau age of 44.88 ± 0.51 Ma. Dated grains were large (~1 mm), characteristic of biotite formed in the dextral strain shadows of amphibole or feldspar porphyroclasts in the

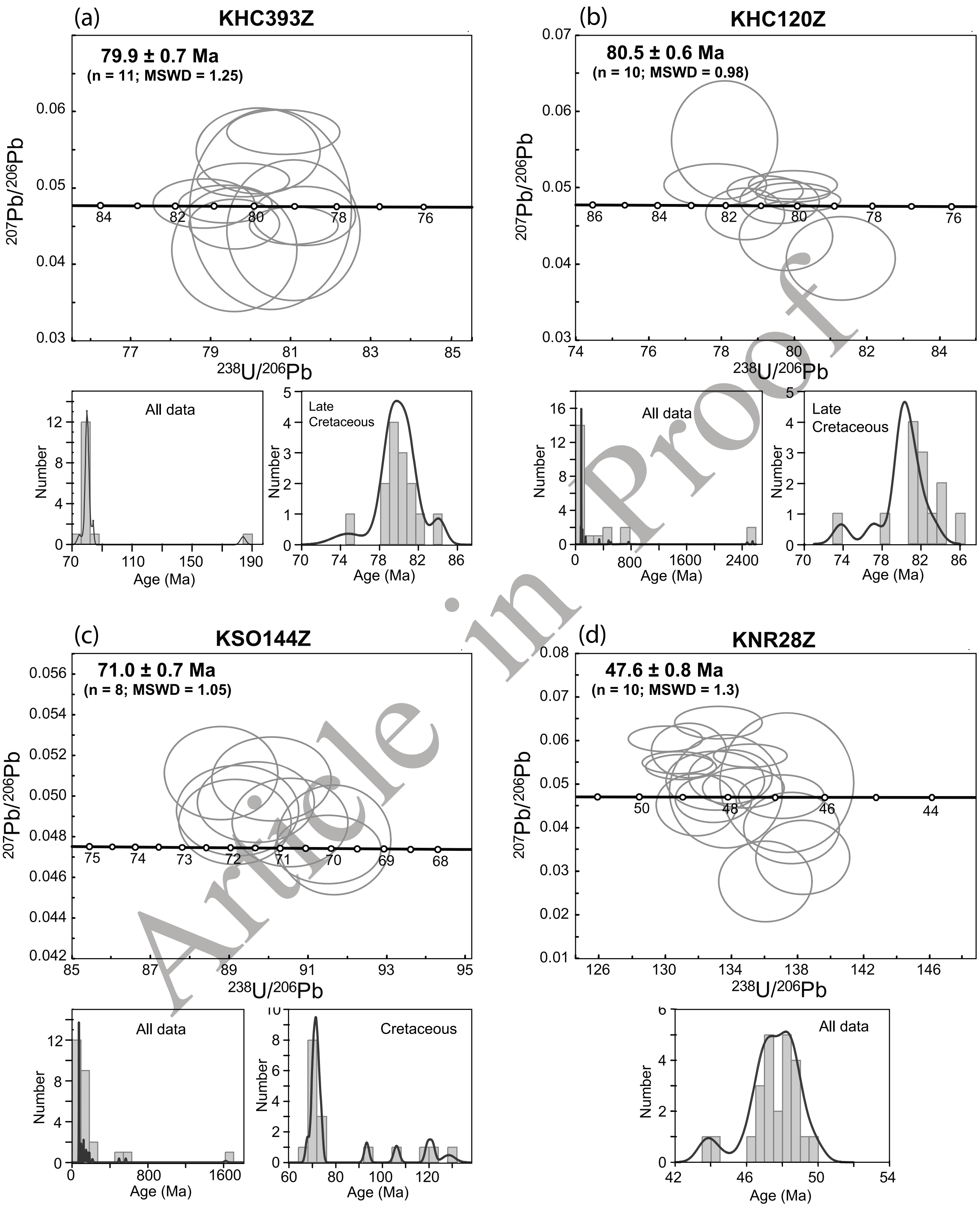

Figure 5. Tera-Wasserburg U-Pb zircon concordia plots for samples (a) KHC393Z, (b) KHC120Z, (c) KSO144Z, and (d) KNR28Z. Error ellipses are one sigma. Small graphs show age histograms against number of analyses, and cumulative probability plots (black line) for all analyses.

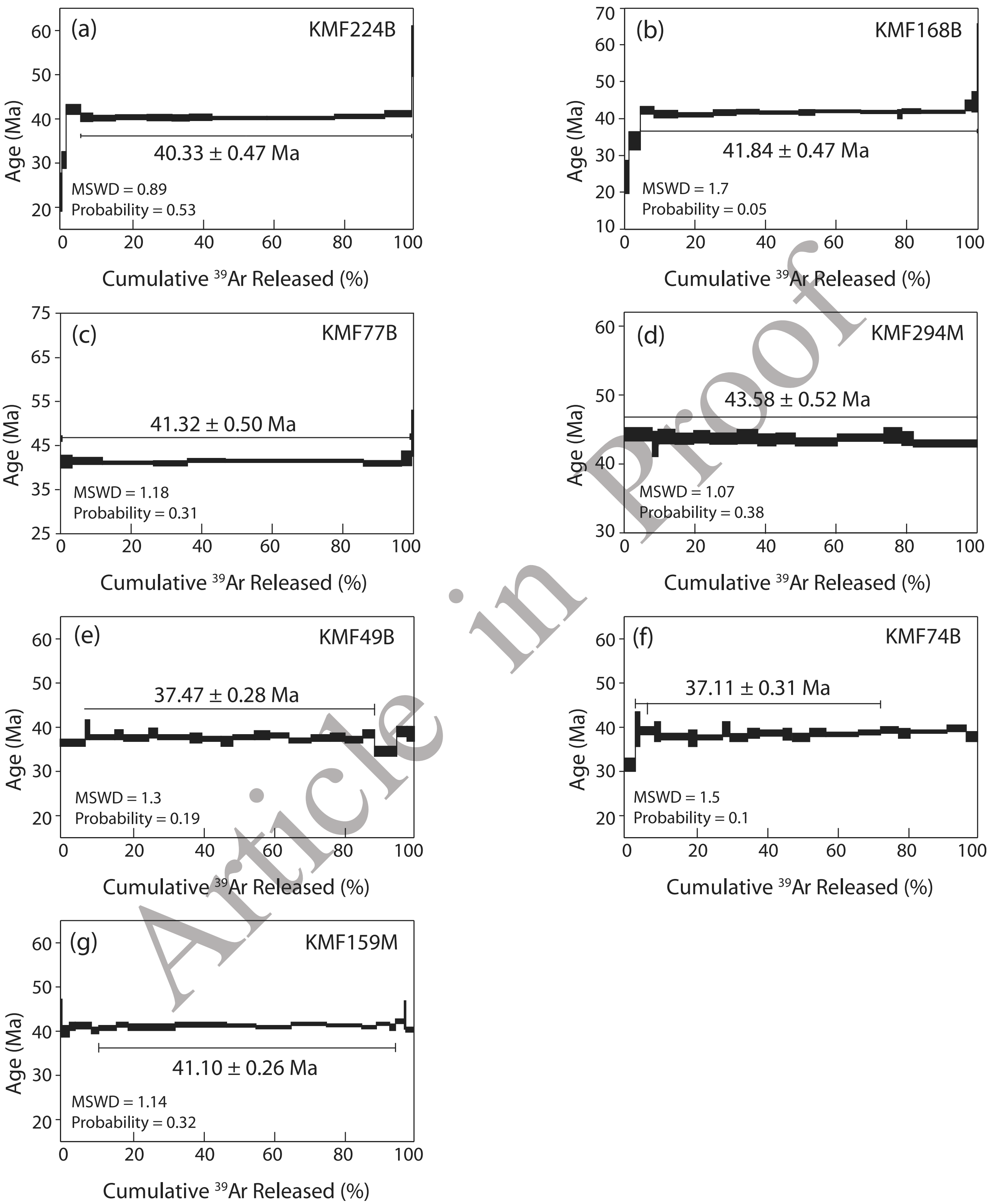

Figure 6. The $^{40}Ar/^{39}Ar$ gas release spectra for samples from the Khlong Marui Fault. See Table 2 and text for details.

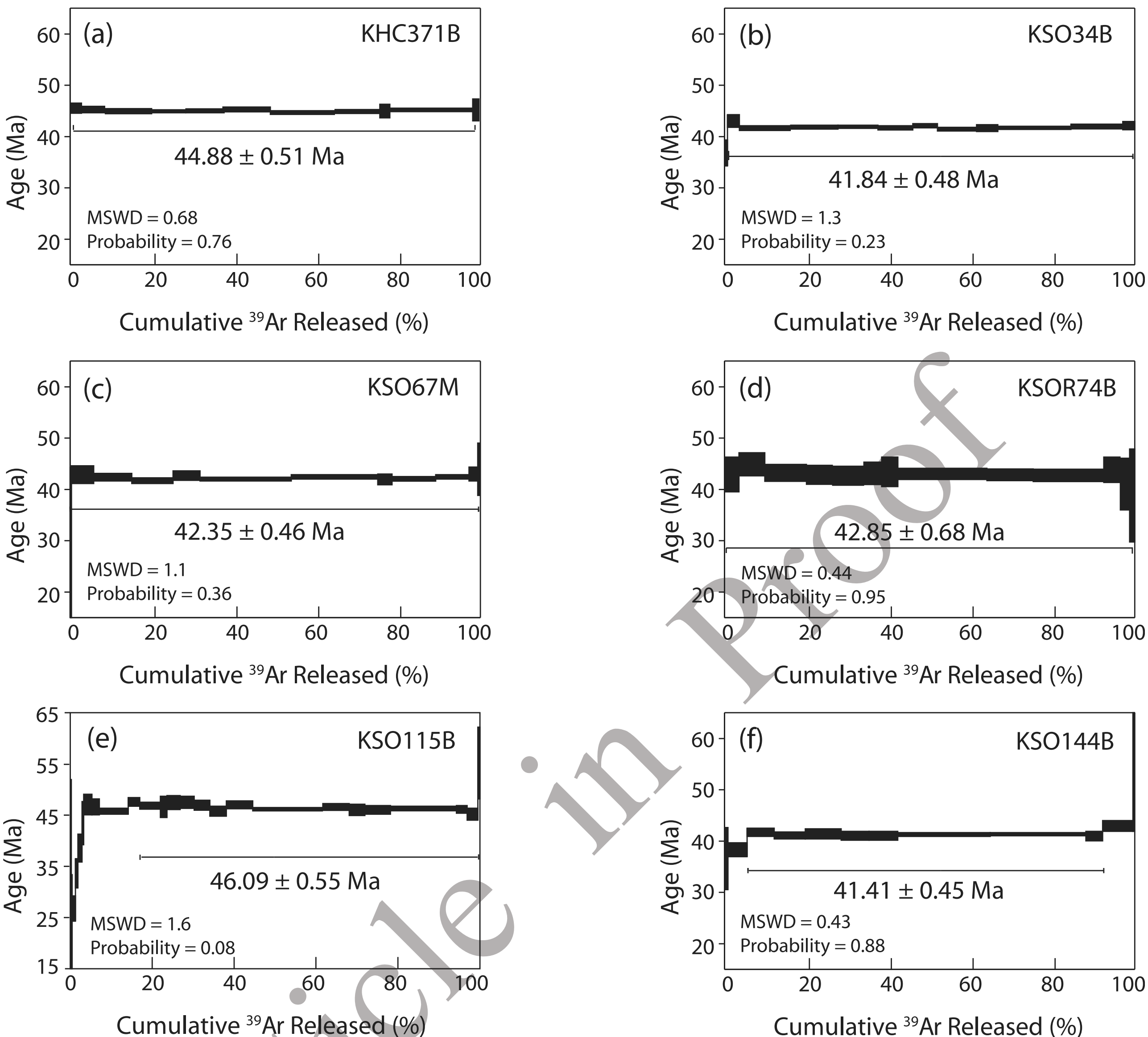

Figure 7. The $^{40}Ar/^{39}Ar$ gas release spectra for samples from the southern Ranong Fault. See Table 2 and text for details.

sample, rather than the much finer biotite of the matrix. Biotite grains taper from an attachment point on the porphyroclast, with a dextral stair-stepping geometry (Figure 10a). Similar large biotites are associated with complex fragmented porphyroclasts, and their mode of formation is a combination of strain shadow and inter-boudin growth. Such grains must have grown during dextral shear, because porphyroclasts and porphyroclast boudins would not have been foci for asymmetric biotite growth before shear, and inter-boudin space would not have existed. We interpret $^{40}Ar/^{39}Ar$ plateau ages from such grains to be equal to, or younger than the age of ductile dextral shear, which, in the Khao Pho Ta Chong Dong area of the RF must have occurred at or before 44.88 ± 0.51 Ma.

5.2. Khao Sai On Ductile Fault Core (Ranong Fault)

[37] The central part of the RF is dominated by a belt of strongly sheared biotite granite at least 35 km long (it extends into Myanmar and may be more than twice as long) and 2.5 km wide, centered on Khao Sai On (Figure 2). Mylonitic fabrics are pervasive, and include a sub-vertical NNE striking foliation and a sub-horizontal lineation. Kinematic indicators show dextral shear. Muscovite-feldspar pegmatite veins within the granite preserve similar fabrics.

[38] Twenty six SHRIMP analyses on 21 zircon grains from sample KSO144Z, typical of the Khao Sai On mylonitic granite, yielded a large range of ages from ~70 Ma to >1.6 Ga. The youngest ages cluster strongly, and correspond to grain rims. Omitting one (#10–1) as a statistical outlier yields an age of 71.0 ± 0.7 Ma (2; n = 8; MSWD = 1.05) for this group, which we consider to represent the emplacement age of the granite. It is younger than the Ranong and Khao Hin Chang granites, but may reflect a common link to the same Late Cretaceous magmatic episode. No undeformed part of the granite body lies outside the shear zone, but solid state deformation fabrics show that this body was intruded

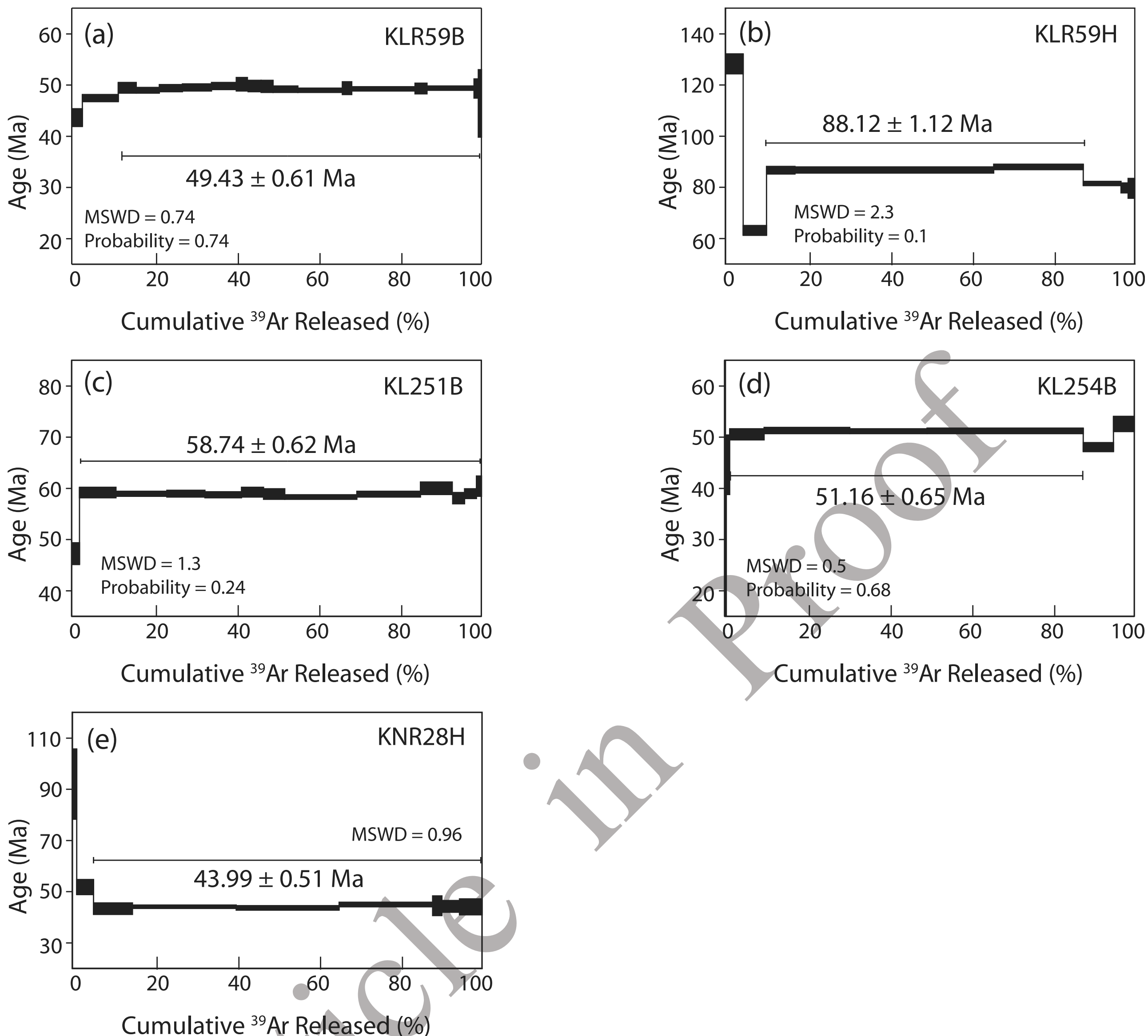

Figure 8. The $^{40}Ar/^{39}Ar$ gas release spectra for samples from the northern Ranong Fault. See Table 2 and text for details.

and crystallized before dextral shear began. The granite has a locally inter-fingering, gradational or sheared relationship with a belt of migmatites, which are also pre-kinematic with respect to ductile dextral shear.

[39] Large biotite grains in sample KSO144B are concentrated within dextral shear planes (Figure 10b). Their large size relative to fine matrix biotite shows that they grew in situ, and are not simply rotated matrix grains, while their restriction to dextral shear planes indicates that they grew during this phase of deformation. Biotite grains selected for dating are comparable in size to the shear band micas, and we infer that our results relate implicitly to this coarser grain population. These coarse biotite grains yielded an $^{40}Ar/^{39}Ar$ plateau age of 41.41 ± 0.45 Ma, indistinguishable from the structurally identical KSO34B (41.84 ± 0.48 Ma), from the same sheared granite body 17 km to the south. Both samples also show a younger first heating step between 30 Ma and 40 Ma, indicating the possibility of a minor thermal overprint at this time.

[40] Sample KSO67M (Figure 10c) is a stretched pegmatite vein in quartz-biotite mylonite country rock adjacent to the sheared granitoid discussed above. Muscovite from large mica fish in this sample yielded an $^{40}Ar/^{39}Ar$ plateau age of 42.35 ± 0.46 Ma. Large biotite fish in sample

Figure 9. Sketch map and cross section showing the relative timing of tectono-magmatic events close to Ranong town. Dextral shear zone (1) is truncated by the Late Cretaceous Ranong Granite (2), which is itself deformed by a post-intrusion shear zone (3) in the NW. Sinistral offset between the granite body (2) and the dextral shear zone (3) is a result of later slip along sinistral brittle faults (4). Position of E-W section A-A′ marked on map. See text for details, and Figure 2 for location.

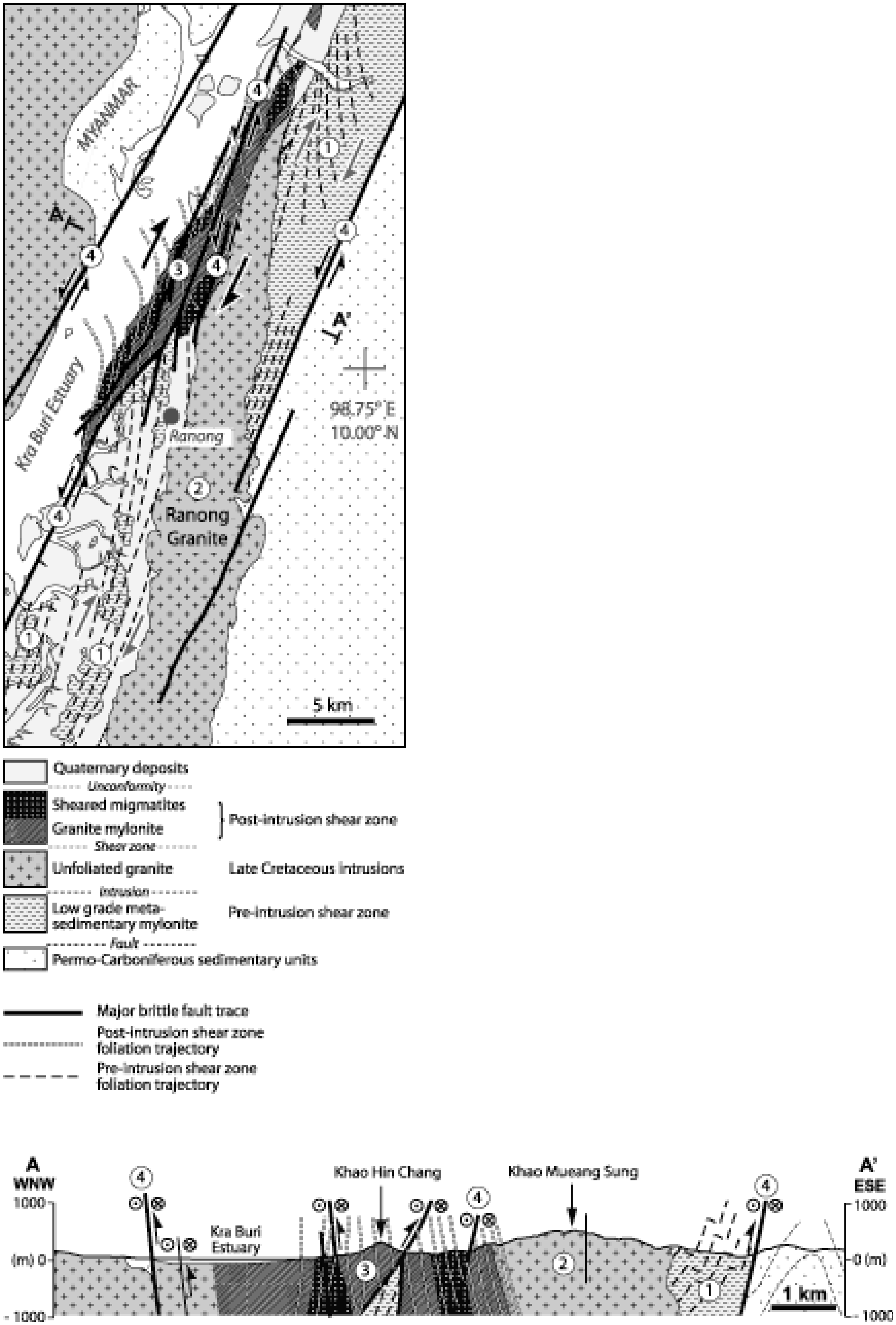
MYANMAR
A
A'
Kra Buri Estuary
Ranong
Ranong Granite
98.75° E
10.00° N
5 km
Quaternary deposits
Unconformity
Sheared migmatites
Granite mylonite
Post-intrusion shear zone
Shear zone
Unfoliated granite
Late Cretaceous intrusions
Intrusion
Low grade meta-sedimentary mylonite
Pre-intrusion shear zone
Fault
Permo-Carboniferous sedimentary units
Major brittle fault trace
Post-intrusion shear zone foliation trajectory
Pre-intrusion shear zone foliation trajectory
A WNW
A' ESE
Khao Hin Chang
Khao Mueang Sung
Kra Buri Estuary
1000
(m) 0
- 1000
1 km

Figure 9

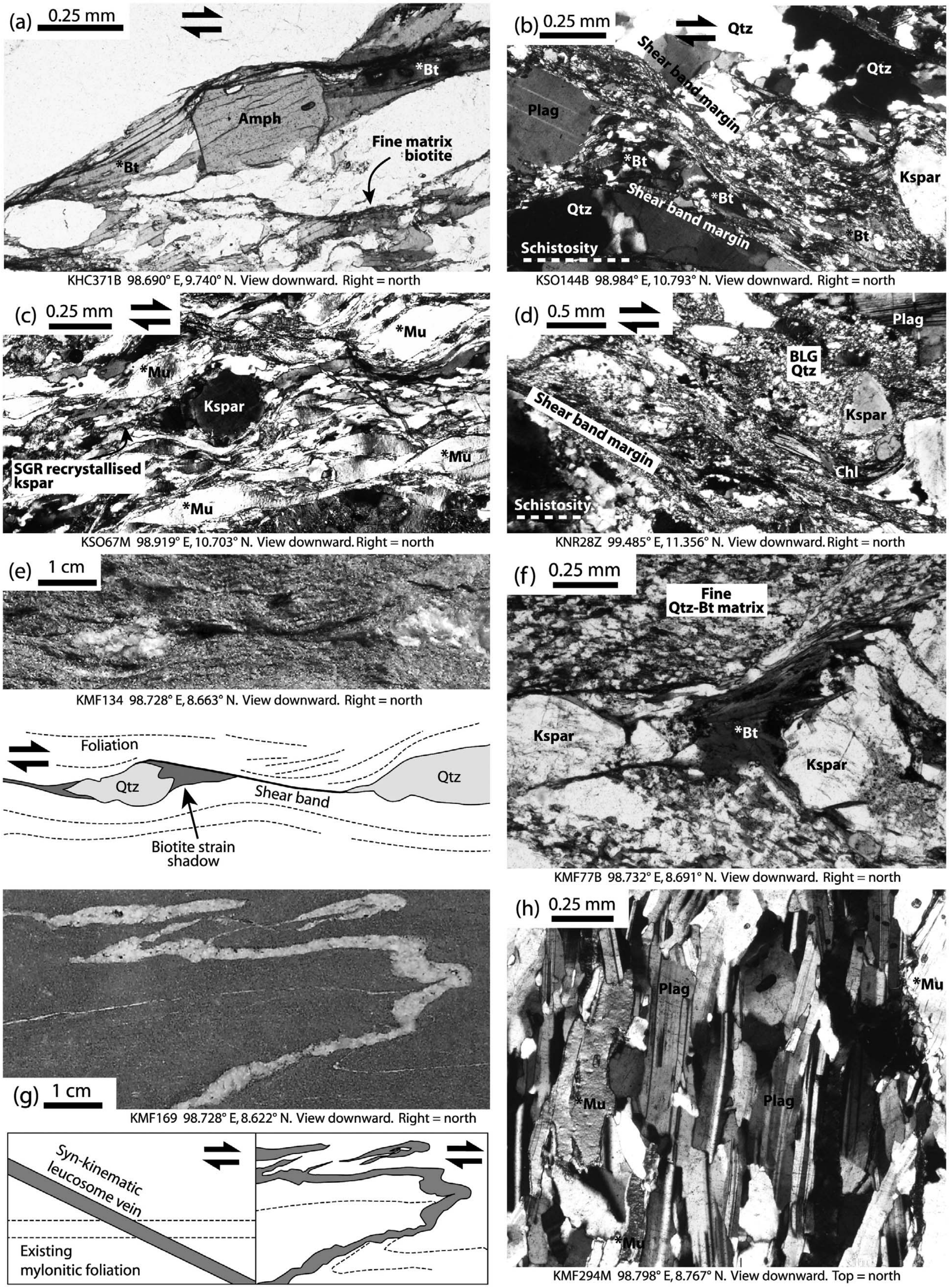

(a) 0.25 mm
Amph
*Bt
Fine matrix biotite
KHC371B 98.690° E, 9.740° N. View downward. Right = north
(b) 0.25 mm
Qtz
Shear band margin
Plag
Kspar
*Bt
Schistosity
KSO144B 98.984° E, 10.793° N. View downward. Right = north
(c) 0.25 mm
*Mu
Kspar
SGR recrystallised kspar
KSO67M 98.919° E, 10.703° N. View downward. Right = north
(d) 0.5 mm
Plag
BLG Qtz
Kspar
Shear band margin
Chl
Schistosity
KNR28Z 99.485° E, 11.356° N. View downward. Right = north
(e) 1 cm
KMF134 98.728° E, 8.663° N. View downward. Right = north
Foliation
Qtz
Shear band
Biotite strain shadow
(f) 0.25 mm
Fine Qtz-Bt matrix
Kspar
*Bt
KMF77B 98.732° E, 8.691° N. View downward. Right = north
(g) 1 cm
KMF169 98.728° E, 8.622° N. View downward. Right = north
Syn-kinematic leucosome vein
Existing mylonitic foliation
(h) 0.25 mm
Plag
*Mu
KMF294M 98.798° E, 8.767° N. View downward. Top = north

Figure 10

KSOR74B from the mesosome of a migmatite band closely associated with the sheared Late Cretaceous intrusion yielded an $^{40}Ar/^{39}Ar$ plateau age of 42.85 ± 0.68 Ma. In both samples KSO67M and KSOR74B, the mica fish are discrete and coarse grained (>0.5 mm) in comparison to fine matrix micas, making them easy to isolate during mineral separation.

[41] Unlike large mica growths discussed previously and inferred to be syn-kinematic, mica fish represent pre-kinematic porphyroclasts deformed by rotation, dislocation glide, erosion and recrystallization, or separation along antithetic microfaults [e.g., *Lister and Snoke*, 1984; *Mares and Kronenberg*, 1993], and may retain older ages. However, the $^{40}Ar/^{39}Ar$ ages of mica fish are similar to the ages of syn-kinematic mica growth in structurally comparable units, and significantly different to the inferred Late Cretaceous age of anatexis and granite emplacement. Both pre- and syn-kinematic micas are therefore inferred to have had their $^{40}Ar/^{39}Ar$ systematics completely reset during or after shear, with the plateau ages obtained taken to represent a youngest limit on the timing of ductile shear.

[42] A sliver of unfoliated biotite granite about 15 × 1.5 km in map view lies west of the large mylonitic granite belt at Khao Sai On (Figure 2). Its $^{40}Ar/^{39}Ar$ plateau age of 46.09 ± 0.55 Ma (KSO115B) indicates that it was emplaced and cooled before the middle Eocene. The young early heating steps from this sample may represent argon loss in the outer rim of the grains due to weathering, but may also indicate that it was a cool, rigid fragment that acted as an undeformed mega-porphyroclast that suffered some heating during post-emplacement ductile deformation in the adjacent dextral shear zone.

5.3. Khao Lat Ductile Fault Core (Ranong Fault)

[43] North of the Khao Sai On ductile fault core, small biotite granite plutons are exposed within a lenticular belt of sheared migmatites, granites and quartzites 30 × 6 km in map section, centered on Khao Lat (Figure 2). The unfoliated granites may have the same structural setting as the Khao Sai On unfoliated granite (KSO115B). Biotite sample KL251B from an undeformed granite near Khao Lat yielded a biotite $^{40}Ar/^{39}Ar$ plateau age of 58.74 ± 0.62 Ma. This may reflect slow cooling to ~350° following emplacement during the Late Cretaceous magmatic event observed in zircon samples from Khao Sai On, Khao Hin Chang and near Ranong town.

[44] Garnet and sillimanite bearing migmatites adjacent to the undeformed granite near Khao Lat preserve relatively poorly developed mylonitic fabrics and dextral kinematic indicators, and their orientation is more variable than elsewhere within the RF. Biotite from these migmatites yielded $^{40}Ar/^{39}Ar$ plateaux at 51.16 ± 0.65 Ma (KL254B) and 49.43 ± 0.61 Ma (KLR59B). Hornblende sample KLR59H from the same migmatite at Khao Lat yielded an older $^{40}Ar/^{39}Ar$ plateau age of 88.12 ± 1.12 Ma. These ages suggest that the Khao Lat migmatites formed and crystallized in the Late Cretaceous, at the same time as the Ranong and Khao Sai On granites, but that they have not been significantly thermally disturbed since their last major cooling event at ~49 to ~51 Ma.

[45] The first heating step in the KLR59B gas release spectrum is about 44 Ma, suggesting a slight thermal event at the same time or just before many other biotite plateau ages from the RF and KMF. Dextral mylonitic microstructures including feldspar recrystallization in the migmatite are similar to most other mylonites from the RF. However, elsewhere in the RF these fabrics are associated with well defined plateau ages in biotite, rather than younger early heating steps. Dextral deformation in the Khao Lat migmatites must therefore have occurred after their Late Cretaceous (88.12 ± 1.12 Ma.) formation, and before their undisturbed ~49 to ~51 Ma biotite $^{40}Ar/^{39}Ar$ plateaux.

5.4. Khao Nakkharat Ductile Fault Core (Ranong Fault)

[46] Pervasive, intense, solid state dextral mylonitic fabrics exist throughout an elongate granitoid body (at least 1 × 14 km in map section) at Khao Nakkharat (Figure 2), near the northern end of the RF. The rock is a coarse grained porphyritic mylonitic/protomylonitic granite, essentially an augen gneiss, dominated by sigma-type porphyroclasts of pale pink K-feldspar. Fine grained biotite, chlorite and hornblende form the dark portions of the matrix, and augment the steeply dipping gneissic foliation. Sub-horizontal lineations and dextral shear sense indicators are widespread.

[47] Shear sense, orientation, style and scale of deformation are similar to mylonitic granites at Khao Hin Chang and Khao Sai On, and solid state mylonitic fabrics in the granite and adjacent migmatites show that they too are pre-kinematic with respect to dextral ductile shear.

[48] Twenty four SHRIMP analyses were made on 17 zircon grains from sample KNR28Z, representative of the Khao Nakkharat mylonitic granite. Three analyses were of grain cores, and fourteen of rims. Core and rim ages were indistinguishable (Figure 4d) in a relatively dispersed data set, although the spread in ages for the entire population (i.e., MSWD = 6.7, n = 24) indicate geological complexity. The other samples of this study all show zircon inheritance, and it is probable that some of the older analyses reflect a xenocrystic component which may only be a few million years older than the emplacement age. Deleting the older analyses progressively does not lower the MSWD to the level which would suggest a single aged population because the youngest

Figure 10. Evidence of the relative age of dated minerals. (a) Sample KHC371B, large syn-kinematic biotite grains in asymmetric pressure shadows around an amphibole porphyroclast. (b) Sample KSO144B, large syn-kinematic biotite grains within a shear band. (c) Sample KSO67M, large pre-kinematic muscovite grains deformed into fish. (d) Sample KNR28H, quartz bulging recrystallization within a shear band, indicating shear at temperatures below amphibole closure to Ar diffusion. (e) Quartz boudins, showing asymmetric syn-kinematic biotite strain shadows. (f) Syn-kinematic biotite growth between two asymmetric quartz-feldspar boudins. (g) Inter-kinematic granitoid vein. Interpretation on the left shows a vein cutting an existing dextral mylonitic foliation (revealed in thin section). Interpretation on the right shows the foliation and crosscutting vein folded by continued dextral shear. (h) Sample KMF294M, syn-kinematic magmatic mica in a muscovite-feldspar vein.

two analyses (#3–1 and #4–1) are statistical outliers to the remainder of the analyses. Omitting these two and culling the older analyses progressively results in an age of 47.4 ± 0.5 Ma (2σ; n = 16; MSWD = 1.2).

[49] The reason for the youngest two analyses being discrepant from the others is not obvious, although one has a relatively high common Pb correction (Table 1). Lead loss during an overprinting event is suspected, in which case other analyses may also be affected. Omitting the five youngest analyses as notionally suffering partial Pb-loss, and the two oldest analyses yields an age of 47.9 ± 0.5 Ma (2σ; n = 17; MSWD = 1.4). This result allows for a possible Pb-loss event as well as inheritance. Although these two calculated ages overlap, it is not possible to choose between them and a combined estimate of 47.6 ± 0.8 Ma (2σ) is preferred for the emplacement age of this rock.

[50] Regardless of how it is calculated, the Khao Nakkharat granite emplacement age is significantly younger than the Ranong, Khao Hin Chang and Khao Sai On pre-kinematic granites (KHC393Z, KHC120Z and KSO144Z). However, there is no microstructural evidence for temperatures during deformation having been sufficiently high to affect pre-existing magmatic zircons, so it must be concluded that substantial dextral shear occurred after its 47.6 ± 0.8 Ma emplacement.

[51] Magmatic hornblende from the same sample (KNR28H) yielded an $^{40}Ar/^{39}Ar$ plateau at 43.99 ± 0.51 Ma, indicating cooling of the rock through ~500°C. It is unlikely that this age represents crystallization of the hornblende because it is about 4 My after emplacement of the granite.

[52] Extensive syn-kinematic bulging recrystallization in feldspars within the primary foliation shows that temperatures during shear were moderately hot (~400–600°C [*Passchier and Trouw*, 2005]) and may have at least partially reset the magmatic hornblende's $^{40}Ar/^{39}Ar$ system. However, this sample's argon plateau is so well defined, it must be assumed that total resetting occurred, and that the plateau age represents cooling at the end of high temperatures. The higher temperature schistosity in this sample is overprinted by lower temperature shear planes, forming a pervasive S-C′ fabric. Bulging recrystallization of quartz, and chlorite growth within dextral shear planes (Figure 10d) indicates that they formed during retrograde dextral shear, after or during the cooling event at 43.99 ± 0.51 Ma.

[53] These data show that dextral shear at the northern end of the RF occurred after granite emplacement at 47.6 ± 0.8 Ma. Hornblende cooling at 43.99 ± 0.51 Ma reflects the end of moderately high temperature dextral shear, and the onset of retrograde dextral shear. It thus provides the first constraint on the absolute timing of ductile dextral shear.

5.5. Khao Phanom Ductile Fault Core (Khlong Marui Fault)

[54] Mylonites associated with the KMF are exposed within a ductile fault core centered on Khao Phanom (Figure 2). They are composed of migmatites, phyllonites, quartzites and mylonitic granites. Biotite samples KMF49B and KMF168B are from structurally identical phyllonitic migmatite mesosomes. They yielded $^{40}Ar/^{39}Ar$ plateaux at 37.47 ± 0.28 Ma and 41.84 ± 0.47 Ma respectively. The migmatites are sillimanite bearing, and it is considered that they form part of the same pre-kinematic basement complex as the RF migmatites. Biotite grains are large throughout the rock, so it is unclear whether dated grains are of syn-kinematic or pre-kinematic origin. Younger ages of 20–35 Ma in the first two heating steps of KMF168B indicate possible minor thermal disturbance after the main period of cooling.

[55] Fine grained quartz-biotite mylonites that lack sillimanite and melt veins, but are otherwise similar to the nearby migmatitic phyllonites, form a 22 × 1.5 km band at the western edge of Khao Phanom. Dynamically recrystallized quartz dominates, and forms distinctive sigmoidal segregations that indicate dextral shear. Biotite in the sample has a bimodal size distribution. Grains <63 μm are uniformly distributed throughout, and are probably a metamorphic product of the muddy matrix in the protolith. Larger grains, up to 0.25 mm, lie parallel to the foliation and define a dextral S-C′ fabric. They are particularly large within the spaces formed between separated asymmetric quartz boudin elements stretched parallel to the mylonitic lineation (Figure 10e). Their long axes connect or point toward the ends of adjacent boudin elements (Figure 10f), showing that they grew during boudin separation, and are not a post-kinematic fill or replacement. Such grains must have grown during dextral shear if the boudins are asymmetric and indicate dextral shear, because the space they occupy would not have existed before boudinage. Therefore ages obtained from these grains cannot pre-date shear. Only biotite grains larger than a 63 μm mesh were selected for dating, yielding an $^{40}Ar/^{39}Ar$ plateau at 41.32 ± 0.50 Ma, interpreted to be equal to or younger than the age of ductile dextral shear.

[56] Weakly sheared muscovite-garnet-tourmaline granitoid veins are common within mylonitic rocks along the eastern edge of Khao Phanom. Many are inter-kinematic with respect to dextral shear (i.e., intruded and crystallized between two shear events), distinguished as follows (Figure 10g): (1) formation of a mylonitic fabric during early shear, (2) intrusion of the vein oblique to the early mylonitic fabric, followed by vein crystallization, and (3) resumption of shear, causing asymmetric folding and boudinage of the vein and early mylonitic foliation.

[57] The only difference between a vein formed in this way and a true syn-kinematic vein is that the vein did not crystallize while shear was underway. However, the short time required for small veins to crystallize may still mean that these veins record the timing of intermittent slip along a shear zone that was continuously active on a geological time scale.

[58] Large muscovite grains from a weakly sheared inter-kinematic muscovite-garnet-tourmaline granitoid vein (KMF159M) within the migmatite yielded an $^{40}Ar/^{39}Ar$ plateau at 41.10 ± 0.26 Ma. Because of the possibility of reheating and argon diffusion after intrusion, this age is interpreted as being equal to or younger than the age of ductile dextral shear.

[59] Muscovite sample KMF294M is from a <0.5 m wide syn-kinematic granitoid vein from the northern end of Khao Phanom. Its margins are parallel to the mylonitic foliation, and it has a strong planar and linear magmatic fabric consisting of tourmaline, plagioclase and muscovite aligned parallel to the host solid state mylonitic fabric (Figure 10h). The only solid state fabrics within the vein include minor

bulging recrystallization and subgrain rotation of quartz, and gentle boudinage of the vein margins, indicating that it crystallized shortly before the end of dextral shear, in a relatively low temperature metamorphic environment. Boudinage of pre-kinematic veins in the host mylonites is much more intense. Sample KMF294M yielded an $^{40}Ar/^{39}Ar$ plateau at 43.58 ± 0.52 Ma, which must record crystallization, which is younger than the onset of shear because the vein is syn-kinematic, and older than the end of shear, because the weak, low temperature overprint represents continued deformation after cooling below the temperature at which muscovite can accumulate radiogenic ^{40}Ar. Therefore, like sample KNR28H (43.99 ± 0.51 Ma), sample KMF294M is interpreted to record the absolute timing of ductile dextral shear.

[60] Samples from a mylonitic granite belt at the western edge of Khao Phanom yielded biotite $^{40}Ar/^{39}Ar$ plateaux at 37.11 ± 0.31 Ma (KMF74B) and 40.33 ± 0.47 Ma (KMF224B). The granite is pre-kinematic with respect to ductile dextral shear, and experienced significant solid state deformation. Both samples show younger apparent ages (~20–35 Ma) in the first one or two heating steps, pointing to a minor thermal disturbance after the main period of cooling.

6. The Timing of Strike-Slip Faulting

6.1. Main Phase of Ductile Dextral Shear

6.1.1. Upper Age Constraint

[61] The Khao Nakkharat, Khao Hin Chang, and Khao Sai On granites all exhibit similar scales and styles of deformation, with extensive (1–4 km wide and 14–35 km long) belts of pervasive mylonitisation developed during a single main phase of ductile dextral strike-slip, and we consider it probable that this reflects a single deformation phase along the entire RF and KMF (Figures 11 and 12d). The Khao Hin Chang and Khao Sai On granites have Cretaceous emplacement ages (80.5 ± 0.6 Ma and 71.0 ± 0.7 Ma), but the ductile shear episode must also post-date the Khao Nakkharat granite, emplaced at 47.6 ± 0.8 Ma. This is the upper constraint on shear timing (Figure 11).

6.1.2. Lower Age Constraint

[62] An important consideration when dating mylonitic rocks using $^{40}Ar/^{39}Ar$ is whether the results should be interpreted as cooling ages or the age of recrystallization due to deformation. Cooling ages require that the dated mineral formed at a temperature greater than an assumed closure temperature (Tc). The Tc concept [*Dodson*, 1973] considers volume diffusion, for which temperature is the main control, to control isotope mobility. When the mineral cools through Tc (typically 500°C for hornblende, 350°C for muscovite, 300°C for biotite [e.g., *Harrison*, 1981; *Harrison et al.*, 1985; *Hodges*, 1991; *Hames and Bowring*, 1994; *McDougall and Harrison*, 1999]), it becomes closed to argon diffusion and begins to accumulate radiogenic argon and an age.

[63] Conversely, recrystallization due to deformation at temperatures below Tc should record the timing of mineral growth, rather than cooling through Tc [*Dunlap*, 1997; *Bosse et al.*, 2005]. Minerals grown in this way will yield ages that directly date the end of a ductile deformation event [e.g., *Dunlap*, 1997].

[64] However, argon diffusion is complex, particularly in strongly deformed rocks [e.g., *Maluski*, 1978]. For example, mica fish can retain original metamorphic cooling ages in undeformed parts of the grain, but younger ages in parts of the grain in which shear bands form diffusion pathways [*Kramar et al.*, 2001]. In some circumstances crystallization ages may be preserved despite temperatures of 500–600°C sustained for tens of millions of years [*Rodríguez et al.*, 2003]. Post-deformation processes such as hydrothermal fluid circulation may also affect or reset $^{40}Ar/^{39}Ar$ ages [e.g., *Kent and McCuaig*, 1997], so the concept of Tc must be treated with caution.

[65] Mica $^{40}Ar/^{39}Ar$ ages from mylonitic rocks along the RF and KMF fall into three groups: 37–38 Ma, 40–45 Ma (with the majority of ages clustered around 41–43 Ma), and 49–52 Ma. The oldest cluster is localized to the Khao Lat area of the central RF, and the youngest is localized to parts of the KMF close to major brittle fault strands.

[66] Mica fish, inferred to be of pre-kinematic magmatic origin (e.g., KSO67M and KSOR74B, associated with Late Cretaceous intrusions and migmatites), yield middle Eocene plateau ages similar to many ages from micas inferred to be syn-kinematic growths. This suggests that the argon system in the originally Late Cretaceous micas was completely reset during or after shear.

[67] Because pre-kinematic micas were reset during or after shear, it follows that most syn-kinematic metamorphic mica (for example strain shadows, inter-boudin grains, large shear band grains) were similarly open to argon diffusion until a time at or after the end of shear. With the exception of KHC371B (44.88 ± 0.51 Ma), all of the syn-kinematic mica samples from both fault zones yield plateau ages in a tight range between 40.33 ± 0.47 Ma and 41.84 ± 0.48 Ma, similar to the pre-kinematic grains. Cooling of the pre- and syn-kinematic grains must have occurred after ductile shearing, so the youngest age of this population (40.33 ± 0.47 Ma) represents the lower limit on the timing of shear (Figure 11). This limit is independent of assumptions about Tc.

[68] The outlying sample KHC371B comes from an isolated ductile fault core parallel to the main RF, suggesting that the cooling event occurred ~3 Ma before it did in the other ductile fault cores (Figures 2 and 11).

6.1.3. Absolute Age Constraint

[69] Upper and lower constraints bound the timing of ductile shear to between 47.6 ± 0.8 Ma and 40.33 ± 0.47 Ma. These bounds are independent of assumptions about Tc for $^{40}Ar/^{39}Ar$ ages. However, it is possible to further constrain the timing of shear by assuming Tc for the following two samples:

[70] 1. Muscovite from a thin syn-kinematic muscovite-feldspar vein within KMF migmatites (KMF294M) is the only mica sample from the sheared rocks that displays a magmatic cooling age undisturbed by subsequent shear. The strong magmatic fabric of this sample parallel to the host mylonitic fabric shows that it was intruded during dextral shear, so its age cannot predate shear. Very minor solid state deformation occurred during shear under low grade metamorphic conditions, presumably after 'closure' to argon diffusion. The $^{40}Ar/^{39}Ar$ age plateau at 43.58 ± 0.52 Ma must therefore record mica cooling during the late stages

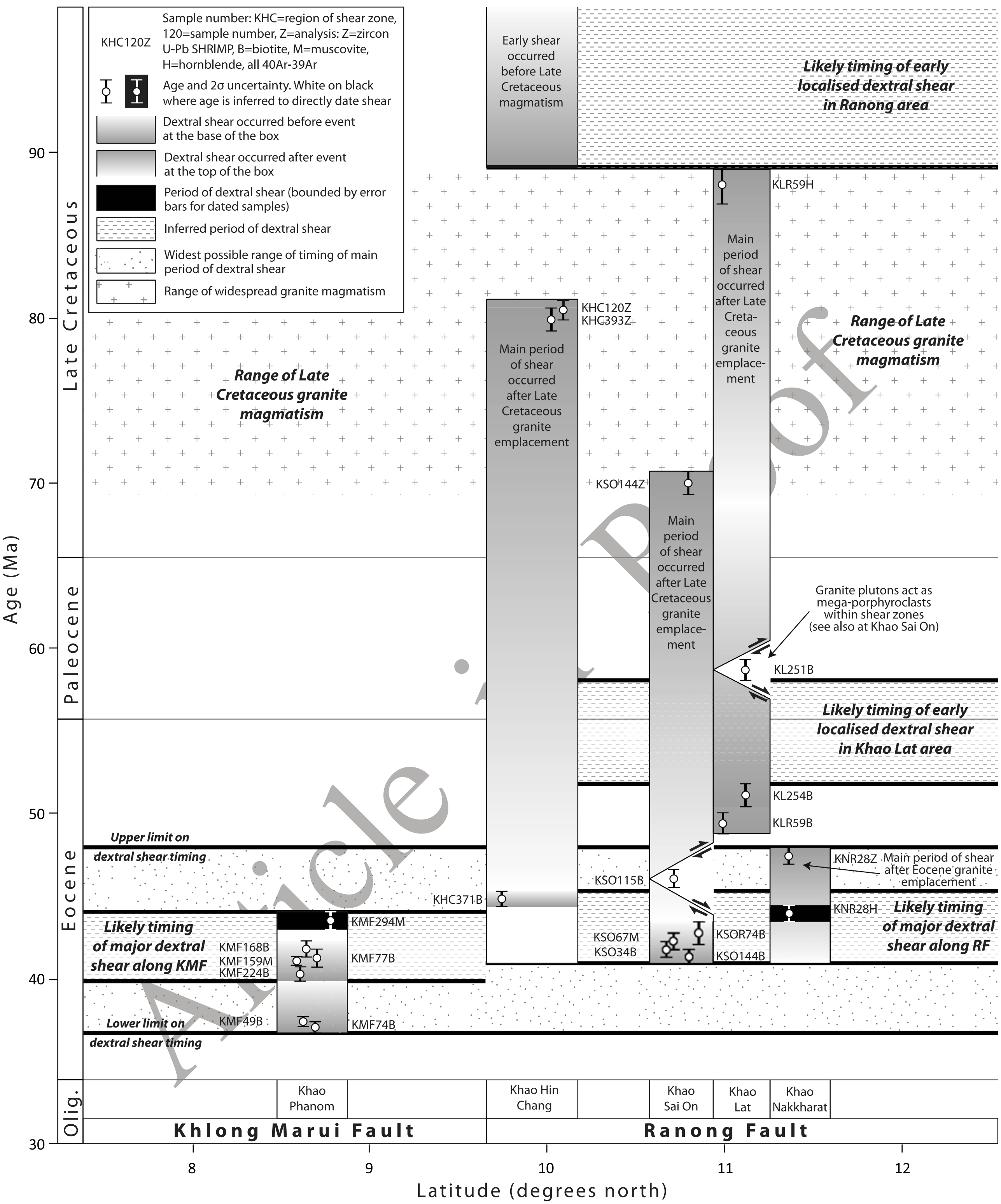

Figure 11. Synthesis of age constraints for periods of shear along the RF and KMF, on age versus latitude axes. See text for explanation.

of shear and crystallization. An unfoliated pegmatite from a similar structural setting near the SE edge of the KMF ductile fault core yielded a similar plateau age (42.59 ± 0.53 Ma [*Charusiri*, 1989]), suggesting that syn-kinematic magmatism was short-lived. Metamorphism, magmatism and associated melting that were synchronous with shear were not caused by shear – i.e., there is no shear heating. These processes merely occurred in an area that was undergoing shearing at the same time, possibly localized by the thermally weakened crust.

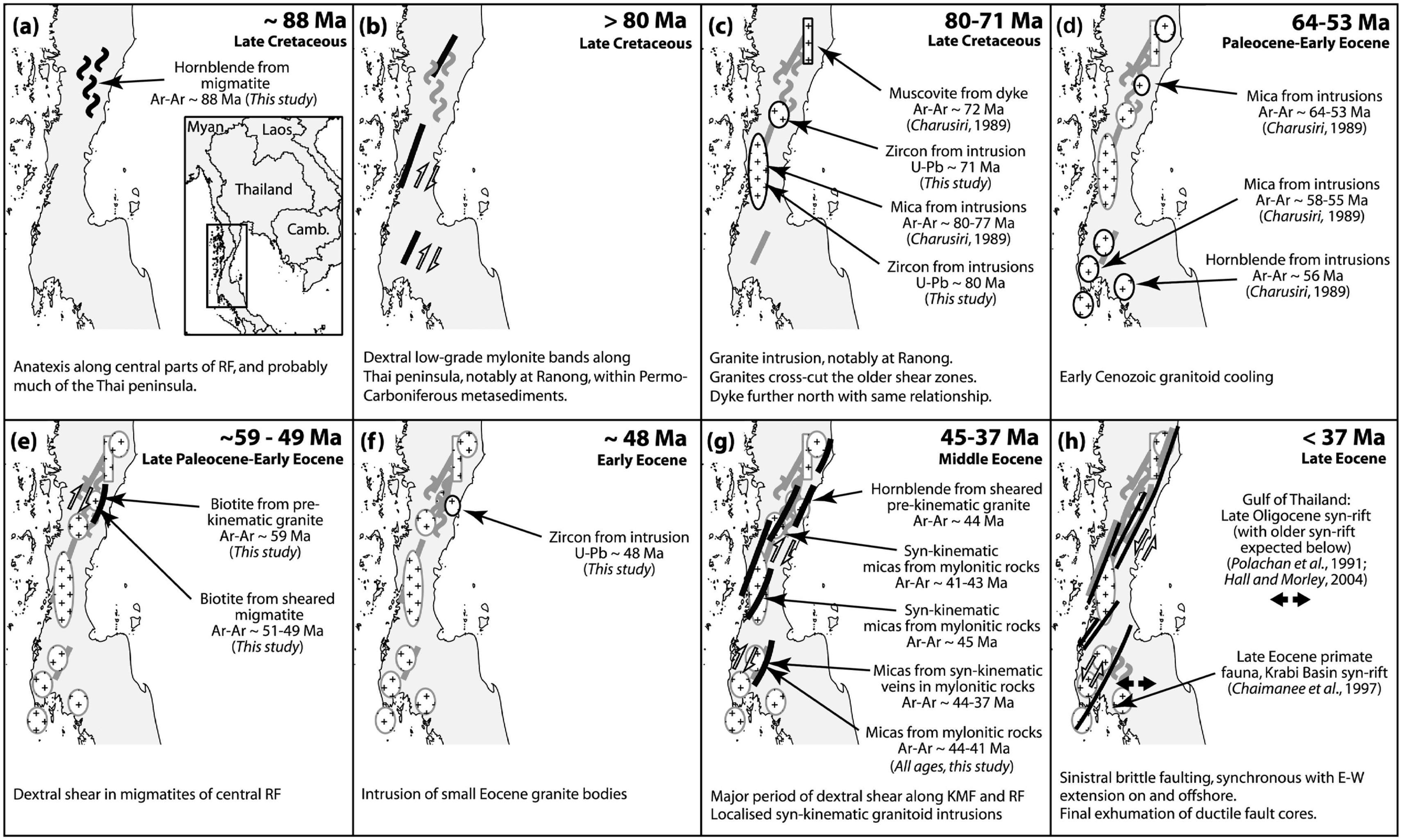

Figure 12. Summary diagrams showing the tectono-magmatic evolution of the Thai peninsula with respect to the Ranong and Khlong Marui faults. See text and individual boxes for explanation.

[71] 2. Bulging recrystallization in mylonitic schistosity-defining feldspars shows that shear occurred before hornblende KNR28H cooled through Tc for argon at 43.99 ± 0.51 Ma. Lower temperature shear planes probably formed after the sample cooled, implying that ductile shear occurred during the cooling that yielded an age of 43.99 ± 0.51 Ma.

[72] Using these constraints, it is possible to conclude that most ductile dextral strike-slip deformation occurred during the middle Eocene within the following constraints (Figures 11 and 12): (1) after emplacement of the Khao Nakkharat granite at 47.6 ± 0.8 Ma (Figure 12f), (2) during cooling of the Khao Nakkharat granite through ~500°C at 43.99 ± 0.51 Ma, (3) during syn-kinematic intrusion at Khao Phanom at 43.58 ± 0.52 Ma to 42.59 ± 0.53 Ma (Figure 12g), (4) before the widespread cooling across both fault zones at 42.85 ± 0.68 Ma to 40.33 ± 0.47 Ma. In the Khao Pho Ta Chong Dong ductile fault core south of Ranong town, cooling occurred about 3 Ma earlier, at 44.88 ± 0.51 Ma, indicating that shear too may have concluded earlier in that ductile fault core (Figure 12g).

6.2. Older Phases of Dextral Shear

[73] Several lines of evidence suggest that an earlier phase of ductile dextral strike-slip shearing preceded the major middle Eocene deformation defined above, and also pre-dated Late Cretaceous granite emplacement in the Ranong area.

[74] Late Cretaceous granite (zircon U-Pb sample KHC393Z: 79.9 ± 0.7 Ma) is cut by a dextral shear zone at Khao Hin Chang (Figure 9). However, the undeformed part of the granite itself cuts through an older shear zone composed of low grade mylonitic meta-sediments, including pebbly mudstones. These rocks are similar to regionally metamorphosed Kaeng Krachan Group metasediments, locally exposed across the Thai peninsula. However, in the Ranong area, steeply dipping mylonitic foliations, gently plunging lineations and dextral kinematic indicators parallel to the trend of the RF are common. The low grade shear zone is sharply truncated by the Ranong granite, and is exposed, undeflected, north and south of the intrusion. There is no evidence of a faulted contact. This relationship suggests a shear-intrusion-shear sequence of events in the Ranong area, summarized below and in Figures 9, 11 and 12:

[75] 1. After Permo-Carboniferous deposition of the Kaeng Krachan Group and before 79.9 ± 0.7 Ma (the zircon U-Pb age of the Ranong granite margin): dextral shearing formed the older, low grade shear zone (Figure 12b).

[76] 2. 79.9 ± 0.7 Ma: Intrusion of the Ranong granite, and truncation of the older shear zone (Figure 12c).

[77] 3. After 79.9 ± 0.7 Ma: dextral shear formed the younger shear zone at Khao Hin Chang. This is most likely to have happened during the middle Eocene, at the same time that similar deformation occurred along the rest of the RF and KMF (Figure 12g).

[78] 4. After middle Eocene shear at Khao Hin Chang: sinistral brittle faulting translated part of the Khao Hin Chang shear zone to the SSW (Figure 12h).

[79] Twenty five kilometers north of Bang Saphan (Figure 2), a post-kinematic unfoliated pegmatite dyke intruded into low grade mylonitic rocks similar to those of the older Ranong shear zone yielded a muscovite $^{40}Ar/^{39}Ar$ plateau at 71.77 ± 0.55 Ma [*Charusiri*, 1989], Figure 12c, indicating that NNE trending dextral shear may have been widespread during or before the Late Cretaceous (Figure 12b).

[80] In the central part of the RF, near Khao Lat, migmatites are of Late Cretaceous age (hornblende $^{40}Ar/^{39}Ar$ plateau at 88.12 ± 1.12 Ma), Figure 12a. Solid state dextral shear fabrics in the migmatite formed at metamorphic conditions similar to mylonites elsewhere along the RF, which mostly yield simple biotite $^{40}Ar/^{39}Ar$ plateaux at about 40–44 Ma. However, biotite $^{40}Ar/^{39}Ar$ ages of 51.16 ± 0.65 Ma and 49.43 ± 0.61 Ma from the Khao Lat migmatites would have been reset by younger middle Eocene shear if it had occurred in the Khao Lat area. Therefore, ductile dextral shear must have occurred in the Khao Lat area no more recently than 51.16 ± 0.65 Ma.

[81] Weak foliation at the margins of a number of porphyritic biotite granite plutons within the Khao Lat migmatites indicates that shear occurred after they were emplaced and cooled sufficiently that they were able to act as rigid mega-porphyroclasts. Their emplacement age is not known, but a biotite $^{40}Ar/^{39}Ar$ plateau of 58.74 ± 0.62 Ma (KL251B) from the center of one of the intrusions is unlikely to have been reset by marginal shear, and so provides a probable upper limit for shear timing (Figure 12e). The sequence of events at Khao Lat can be summarized as follows (Figures 11 and 12): (1) Late Cretaceous (88.12 ± 1.12 Ma to 71.0 ± 0.7 Ma) anatexis and granite emplacement (Figure 12a and 12c). (2) Dextral shear, after Late Cretaceous crystallization of migmatites and granites, probably after late Paleocene (58.74 ± 0.62 Ma) granite cooling, and certainly before early Eocene (51.16 ± 0.65 Ma to 49.43 ± 0.61 Ma) sheared migmatite cooling (Figure 12e). (3) Early Eocene (51.16 ± 0.65 Ma to 49.43 ± 0.61 Ma) sheared migmatite cooling. (4) No significant effects during middle Eocene deformation along the rest of the KMF and RF.

6.3. Brittle Strike-Slip Overprint

[82] Major brittle faults overprint all ductile dextral fabrics and most intrusive rocks along the northern Thai peninsula. Brittle fault strands bound the lenticular ductile fault cores, often dipping toward the ductile rocks (i.e., higher grade rocks in the hanging wall, implying a reverse-slip component). This geometry is consistent with the ductile rocks being uplifted by positive flower structures within anastomosing strike-slip fault strands (Figure 9). Some have a dextral shear sense, many others are sinistral, and in the Ranong area sinistral strands have translated the younger western shear zone about 10 km to the SSW of undeformed parts of its pre-kinematic granite protolith (Figure 9).

[83] All the exposed sinistral faults are upper crustal structures, defined by breccia zones tens of meters wide, narrow bands of foliated gouge and polished fault surfaces. Breccias are composed of sedimentary rock, granitoid and mylonites. Several generations of faulting are common, with younger phases forming more narrow, sharp sided structures, indicating progressive uplift. The brittle faults have orientations very similar to the mylonitic fabric of the ductile fault cores, and it is likely that they exploited the pre-existing foliation. These structures occur within and alongside the ductile fault cores, so they must be younger than the widespread cooling at the end of ductile dextral shear (42.85 ± 0.68 Ma to 40.33 ± 0.47 Ma) (Figure 12h).

[84] The timing of slip along the sinistral brittle structures may be estimated on the basis of the dynamic connection between NNE trending sinistral faulting along the peninsula and Cenozoic E-W extension in onshore and offshore Thai basins, both of which are compatible with a N-S maximum horizontal stress (Sh_{max}). While a mechanical link remains controversial [e.g., *Tapponnier et al.*, 1982; *Polachan et al.*, 1991; *Intawong*, 2006; *Morley and Westaway*, 2006], the basins could not open under the E-W Sh_{max} necessary during dextral shear along the NNE trending faults, making it likely that N-S Sh_{max}, sinistral shear and basin formation were all synchronous.

[85] Syn-rift sedimentation started during the late Eocene to late Oligocene [e.g., *Polachan*, 1988; *Ducrocq et al.*, 1995; *Andreason et al.*, 1997; *Chaimanee et al.*, 1997], soon after the widespread cooling demonstrated by $^{40}Ar/^{39}Ar$ plateau ages presented here. Two biotite samples from KMF mylonites have anomalously young $^{40}Ar/^{39}Ar$ plateau ages (KMF49B, 37.47 ± 0.28 Ma and KMF74B, 37.11 ± 0.31 Ma). Both samples are from locations very close to major brittle fault strands at the margins of the ductile fault core. It is possible that their ages were reset by hot fluid circulation during activity along the brittle faults. Other samples yield younger ages between 30 and 40 Ma in the first few steps of their $^{40}Ar/^{39}Ar$ plateaux, for example KSO144B, KSO34B, and KMF168B, supporting the occurrence of minor but widespread heating during the same event. These ages are consistent with the timing of sinistral faulting inferred from basin opening.

7. Discussion and Conclusions

[86] Data presented here show that during the middle Eocene, the RF and KMF experienced a major period of ductile dextral strike-slip shear after 47.6 ± 0.8 Ma, before 42.85 ± 0.68 Ma to 40.33 ± 0.47 Ma, and probably centered at 43.99 ± 0.51 Ma to 43.58 ± 0.52 Ma. Both shear zones were later reactivated by brittle sinistral faults in the late Eocene to early Oligocene, perhaps between about 30 and 37 Ma.

[87] Ductile deformation along the Mae Ping and Three Pagodas faults of northern Thailand is similar in style to that of the RF and KMF and dominated by wide belts of mid to low metamorphic grade strike-slip mylonites within crystalline basement [*Lacassin et al.*, 1997; *Watkinson et al.*, 2008; *Morley et al.*, 2011]. The Doi Inthanon – Lansang gneisses have been displaced ~150 km by sinistral slip along the Mae Ping and Three Pagodas faults [*Lacassin et al.*, 1997; *Morley et al.*, 2007] (Figure 1), comparable to the combined dextral displacement across the RF and KMF estimated by boudin restoration [*Watkinson*, 2009]. Biotite from Lansang gneiss mylonites within the Mae Ping Fault has yielded $^{40}Ar/^{39}Ar$ ages of 33.1 ± 0.4 Ma to 30.6 ± 0.3 Ma, K-feldspar indicated rapid cooling at ~30.5 Ma, and biotite from the TPF yielded ages of 33.4 ± 0.4 Ma [*Lacassin et al.*, 1997]. *Lacassin et al.* [1997] conclude that the last increments of ductile sinistral slip occurred along the Mae Ping Fault between 32.5 Ma and 30.5 Ma, substantially later than dextral slip along the RF and KMF.

[88] These ages suggest that during the late Eocene to early Oligocene the RF and KMF were not conjugate to the Mae Ping and Three Pagodas faults, but were part of a curved belt of sinistral deformation, of which upper crustal levels are exposed in the Thai peninsula, and mid-crustal levels are exposed in northern Thailand. *Morley et al.* [2007], however, interpret 50–40 Ma exhumation of the Umphan Gneiss in west-central Thailand [*Upton*, 1999] (Figure 1) as due to sinistral motion at a restraining bend of the Mae Ping Fault. Coupled with evidence of Paleocene sinistral transpression accommodated by the Mae Ping and Three Pagodas faults [*Morley*, 2004], it is likely that older phases of sinistral slip along the northern faults did coincide with middle Eocene dextral slip along the RF and KMF.

[89] The age of 'hard' India-Eurasia collision is still uncertain, and estimates range from ~55 - 34 Ma [e.g., *Molnar and Tapponnier*, 1975; *Klootwijk et al.*, 1992; *Searle et al.*, 1997; *Aitchison et al.*, 2007]. At the Indus-Tsangpo Suture in the western Himalayas and northern Indian margin, it has been constrained to early Eocene (50.5 Ma) [e.g., *Rowley*, 1998; *Zhu et al.*, 2005; *Green et al.*, 2008], but the timing in the east is less clear. However, widespread Paleocene-Oligocene metamorphism and transpression in Myanmar and west Thailand are consistent with initial coupling between West Burma and India at about 50 Ma [*Morley*, 2004; *Searle et al.*, 2007; *Searle and Morley*, 2011], indicating that the effects of the Indian plate were being transmitted from Sundaland's margin to its interior from that time. The orientation and shear sense of the RF and KMF alone, or as a conjugate pair with the Mae Ping and Three Pagodas faults, are entirely consistent with NE directed compression caused by India coupling to West Burma, particularly when Neogene dextral slip along the Sagaing Fault is restored.

[90] Sinistral brittle reactivation of the RF and KMF at the same time as late Eocene to early Oligocene ductile sinistral slip along the Mae Ping and Three Pagodas faults can be explained if the peninsular faults were reactivated as curved splays, dissipating a component of sinistral displacement that resulted from true extrusion-driven slip along the northern faults.

[91] Pre-Cenozoic dextral shear along the RF clearly predates the approach of India to Asia. While it is not clear how widespread or extensive the older dextral shear was, it is likely that it developed during the Late Cretaceous phase of metamorphism and inferred crustal thickening observed in Myanmar and western Thailand [e.g., *Cobbing et al.*, 1986; *Putthapiban*, 1992; *Charusiri et al.*, 1993; *Mitchell*, 1993; *Barley et al.*, 2003; *Searle et al.*, 2007]. *Watkinson et al.* [2008] discussed a number of tectonic models for Late Cretaceous dextral shear, including subduction of an Indian Ocean dextral transform zone in the Sunda Trench along strike from the RF and KMF. NNE trending, steeply dipping fabrics formed during Late Cretaceous shear, coupled with weakening from subsequent anatexis and magmatism would have aided reactivation of the fault zones during India-West Burma coupling in the Eocene. *Morley et al.* [2011] suggest that strike-slip deformation, basin inversion and metamorphic core complex development were focused in Thailand and eastern Myanmar because hot lower-middle crust in this area was capable of flow following prolonged Mesozoic subduction and magmatism, unlike the stronger crust of western Myanmar.

[92] We conclude that the Ranong and Khlong Marui faults of the Thai peninsula initiated before ~80 Ma as

dextral strike-slip faults during deformation close to the Late Cretaceous Andean-type western margin of Sundaland. Magmatism and anatexis occurred along the peninsula soon after (~88–71 Ma, Figures 12a–12d), and sporadically until the early Eocene (~48 Ma, Figure 12f). Localized dextral shear affected migmatites of the central RF before the early Eocene (~51 Ma), and probably after the late Paleocene (~59 Ma, Figure 12e).

[93] Both the RF and KMF were thoroughly reactivated during the middle Eocene (between about 48 Ma and 40 Ma, centered on about 44 Ma, Figure 12g) in response to coupling between West Burma and India, experiencing a major period of ductile dextral displacement at the same time as early sinistral slip along the Mae Ping and Three Pagodas faults, and transpression and metamorphism in northern Thailand and eastern Myanmar. The peninsular faults became inactive and cooled rapidly in the middle Eocene (~45–40 Ma). Continued sinistral slip along the northern faults during late Eocene extrusion tectonics (~37–30 Ma, Figure 12h) reactivated the peninsular faults as upper crustal sinistral strands of the Mae Ping and Three Pagodas faults, contributing to uplift of the mylonitic ductile fault cores.

[94] **Acknowledgments.** This work was funded by the SE Asia Research Group at Royal Holloway, University of London, UK. Logistical support in the field was provided by the Department of Geological Sciences, Chiang Mai University, Chiang Mai, Thailand; the Department of Mineral Resources, Bangkok, Thailand; and the Department of Mineral Fuels, Bangkok, Thailand. We would like to thank Mike Cosca at Université de Lausanne for $^{40}Ar/^{39}Ar$ analyses. SHRIMP analyses were carried out at the John de Laeter Centre, Curtin University, which is supported by a university-government consortium and ARC. We are very grateful for constructive comments on the text by Mike Searle, Ed DeWitt, Gordon Lister, and an anonymous reviewer.

References

Aitchison, J. C., J. R. Ali, and A. M. Davis (2007), When and where did India and Asia collide?, *J. Geophys. Res.*, *112*, B05423, doi:10.1029/2006JB004706.

Anczkiewicz, R., G. Viola, O. Müntener, M.F. Thirlwall, I. M. Villa, and N. Q. Quong (2007), Structural and shearing conditions in the Day Nui Con Voi massif: Implications for the evolution of the Red River shear zone in northern Vietnam, *Tectonics*, *26*, TC2002, doi:10.1029/2006TC001972.

Andreason, M. W., B. Mudford, and J. E. S. Onge (1997), Geologic evolution and petroleum system of Thailand Andaman Sea Basins, in *Proceedings of the International Conference on Petroleum Systems of SE Asia and Australasia, Indonesian Petroleum Association*, edited by J. V. C. Howes and R. A. Noble, pp. 337–350, Jakarta, Indonesia.

Barley, M. E., A. L. Pickard, K. Zaw, P. Rak, and M. G. Doyle (2003), Jurassic to Miocene magmatism and metamorphism in the Mogok metamorphic belt and the India-Eurasia collision in Myanmar, *Tectonics*, *22* (3), 1019, doi:10.1029/2002TC001398.

Barr, S. M., A. S. Macdonald, B. V. Miller, P. H. Reynolds, B. P. Rhodes, and B. Yokart (2002), New U-Pb and Ar/Ar ages from the Doi Inthanon and Doi Suthep metamorphic core complexes, northwestern Thailand, paper presented at Symposium on Geology of Thailand, Dep. Min. Res., Bangkok.

Bertrand, G., and C. Rangin (2003), Tectonics of the western margin of the Shan Plateau (central Myanmar): Implications for the India-Indochina oblique convergence since the Oligocene, *J. Asian Earth Sci.*, *21*, 1139–1157, doi:10.1016/S1367-9120(02)00183-9.

Bock, Y., L. Prawirodirdjo, J. F. Genrich, C. W. Stevens, R. Mccaffrey, C. Subarya, S. S. O. Puntodewo, and E. Calais (2003), Crustal motion in Indonesia from Global Positioning System measurements, *J. Geophys. Res.*, *108*(B8), 2367, doi:10.1029/2001JB000324.

Bosse, V., G. Féraud, M. Ballèvre, J.-J. Peucat, and M. Corsini (2005), Rb-Sr and $^{40}Ar/^{39}Ar$ ages in blueschists from the Ile de Groix (Armorican Massif, France): Implications for closure mechanisms in isotopic systems, *Chem. Geol.*, *220*, 21–45, doi:10.1016/j.chemgeo.2005.02.019.

Bunopas, S. (1981), Paleogeographic history of western Thailand and adjacent parts of Southeast Asia: A plate-tectonics interpretation, *Geol. Surv. Pap.*, *5*, 801 pp., Dep. of Min. Resour., Bangkok.

Chaimanee, Y., V. Suteethorn, J.-J. Jaeger, and S. Ducrocq (1997), A Late Eocene anthropoid primate from Thailand, *Nature*, *385*, 429–431, doi:10.1038/385429a0.

Charusiri, P. (1989), Lithophile metallogenic epochs of Thailand: A geological and geochronological investigation, Ph.D. thesis, 819 pp., Queen's Univ., Kingston, Ont., Canada.

Charusiri, P., A. H. Clark, E. Farrar, D. Archibald, and P. Charusiri (1993), Granite belts in Thailand: Evidence from the $^{40}Ar/^{39}Ar$ geochronological and geological synthesis, *J. Southeast Asian Earth Sci.*, *8*, 127–136.

Cobbing, E. J., D. I. J. Mallick, P. E. J. Pitfield, and L. H. Teoh (1986), The granites of the Southeast Asian tin belt, *J. Geol. Soc.*, *143*, 537–550, doi:10.1144/gsjgs.143.3.0537.

Compston, W., I. S. Williams, and C. Meyer (1984), U-Pb geochronology of zircons from lunar breccia 73217 using a sensitive high mass-resolution ion microprobe, *J. Geophys. Res.*, *89*, B525–B534, doi:10.1029/JB089iS02p0B525.

Curray, J. R. (2005), Tectonics and history of the Andaman Sea region, *J. Asian Earth Sci.*, *25*, 187–232, doi:10.1016/j.jseaes.2004.09.001.

Dheeradilok, P., P. Sukawatananant, S. Boripatkoson, V. Tunsuwan, and A. Lumjuan (1985), Amphoe Hua Hin, in *Geological Map of Thailand*, 1:250,000, Dep. of Min. Resour., Bangkok.

Dodson, M. (1973), Closure temperature in cooling geochronological and petrological systems, *Contrib. Mineral. Petrol.*, *40*, 259–274, doi:10.1007/BF00373790.

Ducrocq, S., Y. Chaimanee, V. Suteethorn, and J.-J. Jaeger (1995), Mammalian faunas and the ages of the continental Tertiary fossiliferous localities from Thailand, *J. Southeast Asian Earth Sci.*, *12*, 65–78, doi:10.1016/0743-9547(95)00021-6.

Dunlap, W. J. (1997), Neocrystallization or cooling? $^{40}Ar/^{39}Ar$ ages of white micas from low-grade mylonites, *Chem. Geol.*, *143*, 181–203, doi:10.1016/S0009-2541(97)00113-7.

Dunning, G. R., A. S. Macdonald, and S. M. Barr (1995), Zircon and monazite U-Pb dating of the Doi Inthanon core complex, northern Thailand: Implications for extension within the Indosinian Orogen, *Tectonophysics*, *251*, 197–213, doi:10.1016/0040-1951(95)00037-2.

Fitch, T. J. (1972), Plate convergence, transcurrent faults and internal deformation adjacent to Southeast Asia and the Western Pacific, *J. Geophys. Res.*, *77*, 4432–4460, doi:10.1029/JB077i023p04432.

Fontaine, H., C. Chonglakmani, I. Amnan, and S. Piyasin (1994), A well-defined Permian biogeograpic unit: Peninsular Thailand and northwest Peninsular Malaysia, *J. Southeast Asian Earth Sci.*, *9*, 129–151, doi:10.1016/0743-9547(94)90071-X.

Geological Survey of Japan (1997), Digital geologic map of East and Southeast Asia, *Digital Geoscience Map G-2*, 1:2,000,000, Coord. Comm. for Coastal and Offshore Geosci. Programmes in East and Southeast Asia and Geol. Surv. of Jpn., Ibaraki-ken, Japan.

Gilley, L. D., T. M. Harrison, P. H. Leloup, F. J. Ryerson, O. M. Lovera, and J.-H. Wang (2003), Direct dating of left-lateral deformation along the Red River shear zone, China and Vietnam, *J. Geophys. Res.*, *108* (B2), 2127, doi:10.1029/2001JB001726.

Govers, R., and M. J. R. Wortel (2005), Lithosphere tearing at STEP faults: Response to edges of subduction zones, *Earth Planet. Sci. Lett.*, *236*, 505–523, doi:10.1016/j.epsl.2005.03.022.

Green, O. R., M. P. Searle, R. I. Corfield, and R. M. Corfield (2008), Cretaceous-Tertiary carbonate platform evolution and age of the India-Asia collision along the Ladakh Himalaya, *J. Geol.*, *116*, 331–353, doi:10.1086/588831.

Hall, R. (2002), Cenozoic geological and plate tectonic evolution of SE Asia and the SW Pacific: Computer-based reconstructions and animations, *J. Asian Earth Sci.*, *20*, 353–431, doi:10.1016/S1367-9120(01)00069-4.

Hall, R., and C. K. Morley (2004), Sundaland Basins, in *Continental-Ocean Interactions Within East Asian Marginal Seas*, *Geophys. Monogr. Ser.*, vol. 149, edited by P. Clift, P. Wang, W. Kuhnt, and D. Hayes, pp. 55–85, AGU, Washington, D. C.

Hall, R., B. Clements, and H. R. Smyth (2009), Sundaland: Basement character, structure and plate tectonic development, paper presented at 33rd Annual Convention, Indonesian Pet. Assoc., Jakarta.

Hames, W. E., and S. A. Bowring (1994), An empirical evaluation of the argon diffusion geometry in muscovite, *Earth Planet. Sci. Lett.*, *124*, 161–169, doi:10.1016/0012-821X(94)00079-4.

Harrison, T. M. (1981), Diffusion of ^{40}Ar in hornblende, *Contrib. Mineral. Petrol.*, *78*, 324–331, doi:10.1007/BF00398927.

Harrison, T. M., I. Duncan, and I. McDougall (1985), Diffusion of ^{40}Ar in biotite: Temperature, pressure and compositional effects, *Geochim. Cosmochim. Acta*, *49*, 2461–2468, doi:10.1016/0016-7037(85)90246-7.

Hintong, C., S. Sinskul, and C. Pholprasit (1985), Changwat Phuket, in *Geological Map of Thailand*, 1:250,000, Dep. of Min. Resour., Bangkok.

Hodges, K. V. (1991), Pressure-temperature-time paths, *Annu. Rev. Earth Planet. Sci.*, *19*, 207–236, doi:10.1146/annurev.ea.19.050191.001231.

Imtihanah (2000), Isotopic dating of igneous sequences of the Sumatra Fault System, Masters thesis, 150 pp., Univ. London, London.

Intawong, A. (2006), The structural evolution of Tertiary sedimentary basins in southern Thailand and their relationship to the Khlong Marui Fault, Ph.D. thesis, 417 pp., Univ. London, London.

Jardine, E. (1997), Dual petroleum systems governing the prolific Pattani Basin, offshore Thailand, paper presented at Petroleum systems of S.E. Asia and Australasia Conference, Indonesian Pet. Assoc., Jakarta.

Jolivet, L., O. Beyssac, B. Goffé, D. Avigad, C. Lepvrier, H. Maluski, and T. T. Thang (2001), Oligo-Miocene mid-crustal sub-horizontal shear zone in Indochina, *Tectonics*, *20*, 46–57, doi:10.1029/2000TC900021.

Jourdan, F., and P. R. Renne (2007), Age calibration of the Fish Canyon sanidine $^{40}Ar/^{39}Ar$ dating standard using primary K-Ar standards, *Geochim. Cosmochim. Acta*, *71*, 387–402, doi:10.1016/j.gca.2006.09.002.

Katili, J. A. (1978), Past and present geotectonic position of Sulawesi, Indonesia, *Tectonophysics*, *45*, 289–322, doi:10.1016/0040-1951(78)90166-X.

Kent, A. J., and C. McCuaig (1997), Disturbed ^{40}Ar-^{39}Ar systematics in hydrothermal biotite and hornblende at the Scotia gold mine, Western Australia: Evidence for argon loss associated with post-mineralisation fluid movement, *Geochim. Cosmochim. Acta*, *61*, 4655–4669, doi:10.1016/S0016-7037(97)00350-5.

Klootwijk, C. T., J. S. Gee, J. W. Peirce, G. M. Smith, and P. L. Mcfadden (1992), An early India-Asia contact; palaeomagnetic constraints from Ninetyeast Ridge, ODP Leg 121; with suppl. data 92–15, *Geology*, *20*, 395–398, doi:10.1130/0091-7613(1992)020<0395:AEIACP>2.3.CO;2.

Koppers, A. A. P. (2002), ArArCALC-software for $^{40}Ar/^{39}Ar$ age calculations, *Comput. Geosci.*, *28*, 605–619, doi:10.1016/S0098-3004(01)00095-4.

Kramar, N., M. A. Cosca, and J. C. Hunziker (2001), Heterogeneous $^{40}Ar^*$ distributions in naturally deformed muscovite: In situ UV-laser ablation evidence for microstructurally controlled intragrain diffusion, *Earth Planet. Sci. Lett.*, *192*, 377–388, doi:10.1016/S0012-821X(01)00456-3.

Lacassin, R., H. Maluski, P. H. Leloup, P. Tapponnier, C. Hinthong, K. Siribhakdi, S. Chauaviroj, and A. Charoenravat (1997), Tertiary diachronic extrusion and deformation of western Indochina: Structure and $^{40}Ar/^{39}Ar$ evidence from NW Thailand, *J. Geophys. Res.*, *102*, 10,013–10,037, doi:10.1029/96JB03831.

Leloup, P. H., R. Lasassin, P. Tapponnier, U. Schärer, Z. Dalai, L. Xiaohan, Z. Liangshang, J. Shaocheng, and P. T. Trinh (1995), The Ailao Shan-Red River shear zone (Yunnan, China), Tertiary transform boundary of Indochina, *Tectonophysics*, *251*, 3–84, doi:10.1016/0040-1951(95)00070-4.

Leloup, P. H., N. Arnaud, R. Lacassin, J. R. Kienast, T. M. Harrison, T. T. Phan Trong, A. Replumaz, and P. Tapponnier (2001), New constraints on the structure, thermochronology, and timing of the Ailao Shan-Red River shear zone, SE Asia, *J. Geophys. Res.*, *106*, 6683–6732, doi:10.1029/2000JB900322.

Leloup, P. H., P. Tapponnier, and R. Lacassin (2007), Discussion with M.P. Searle: The role of the Red River shear zone, Yunnan and Vietnam, in the continental extrusion of SE Asia, *J. Geol. Soc.*, *164*, 1253–1260, doi:10.1144/0016-76492007-065.

Lister, G. S., and A. W. Snoke (1984), S-C mylonites, *J. Struct. Geol.*, *6*, 617–638, doi:10.1016/0191-8141(84)90001-4.

Ludwig, K. R. (2001), *SQUID 1.03—A User's Manual*, vol. 2, 17 pp., Berkeley Geochronol. Cent., Berkeley, Calif.

Mahawat, C., A. Tantitamsopon, W. Kaewyana, N. Gitisan, and L. Raksaskulwong (1985), Changwat Chum Phon and Amphoe Kra Buri, in *Geological Map of Thailand*, 1:250,000, Dep. of Min. Resour., Bangkok.

Maluski, H. (1978), Behaviour of biotites, amphiboles, plagioclases and K-feldspars in response to tectonic events with the $^{40}Ar/^{39}Ar$ radiometric method. Example of Corsican granite, *Geochim. Cosmochim. Acta*, *42*, 1619–1633, doi:10.1016/0016-7037(78)90251-X.

Mantajit, N., W. Tantiwanit, L. Raksaskulwong, and Y. Ukakimapan (1985), Changwat Phangnga, in *Geological Map of Thailand*, 1:250,000, Dep. Min. Resour., Bangkok.

Mares, V. M., and A. K. Kronenberg (1993), Experimental deformation of muscovite, *J. Struct. Geol.*, *15*, 1061–1075, doi:10.1016/0191-8141(93)90156-5.

Maung, H. (1987), Transcurrent movements in the Burma-Andaman sea region, *Geology*, *15*, 911–912, doi:10.1130/0091-7613(1987)15<911:TMITBS>2.0.CO;2.

McDougall, I., and T. M. Harrison (1999), *Geochronology and Thermochronology by the $^{40}Ar/^{39}Ar$ Method*, 2nd ed., 269 pp., Oxford Univ. Press, New York.

Metcalfe, I. (1994), Gondwanaland origin, dispersion, and accretion of East and Southeast Asian continental terranes, *J. South Am. Earth Sci.*, *7*, 333–347, doi:10.1016/0895-9811(94)90019-1.

Metcalfe, I. (1996), Pre-Cretaceous evolution of SE Asian terranes, in *Tectonic Evolution of Southeast Asia*, edited by R. Hall and D. Blundell, *Geol. Soc. Spec. Publ.*, 106, 97–122.

Metcalfe, I. (2011), Tectonic framework and Phanerozoic evolution of Sundaland, *Gondwana Res.*, *19*, 3–21, doi:10.1016/j.gr.2010.02.016.

Mitchell, A. G. H. (1993), Cretaceous-Cenozoic tectonic events in the Western Myanmar (Burma)-Assam region, *J. Geol. Soc.*, *150*, 1089–1102, doi:10.1144/gsjgs.150.6.1089.

Molnar, P., and P. Tapponnier (1975), Cenozoic tectonics of Asia: Effects of a continental collision, *Science*, *189*, 419–426, doi:10.1126/science.189.4201.419.

Morley, C. K. (2002), A tectonic model for the Tertiary evolution of strike-slip faults and rift basins in SE Asia, *Tectonophysics*, *347*, 189–215, doi:10.1016/S0040-1951(02)00061-6.

Morley, C. K. (2004), Nested strike-slip duplexes, and other evidence for Late Cretaceous-Palaeogene transpressional tectonics before and during India-Eurasia collision, in Thailand, Myanmar and Malaysia, *J. Geol. Soc.*, *161*, 799–812, doi:10.1144/0016-764903-124.

Morley, C. K., and R. Westaway (2006), Subsidence in the super-deep Pattani and Malay basins of Southeast Asia: A coupled model incorporating lower-crustal flow in response to post-rift sediment loading, *Basin Res.*, *18*, 51–84, doi:10.1111/j.1365-2117.2006.00285.x.

Morley, C. K., M. Smith, A. Carter, P. Charusiri, and S. Chantraprasert (2007), Evolution of deformation styles at a major restraining bend, constraints from cooling histories, Mae Ping Fault Zone, Western Thailand, in *Tectonics of Strike-Slip Restraining and Releasing Bends*, edited by W. D. Cunningham and P. Mann, *Geol. Soc. Spec. Publ.*, 290, 325–349.

Morley, C. K., P. Charusiri, and I. Watkinson (2011), Structural geology of Thailand during the Cenozoic, in *The Geology of Thailand*, edited by M. F. Ridd, A. J. Barber, and M. J. Crow, pp. 273–334, Geol. Soc., London.

Nakornsri, N., C. Udomratn, S. Vimuktanandana, S. Polchan, and D. Luangpitakchumpol (1985), Changwat Ranong, in *Geological Map of Thailand*, 1:250,000, Dep. Min. Resour., Bangkok.

Passchier, C. W., and R. A. J. Trouw (2005), *Microtectonics*, 2nd ed., 366 pp., Springer, Berlin.

Polachan, S. (1988), The geological evolution of the Mergui Basin, SE Andaman Sea, Thailand, Ph.D. thesis, 218 pp., Univ. London, London.

Polachan, S., S. Pradidtan, C. Tongtaow, S. Janmaha, K. Intarawijitr, and C. Sangsuwan (1991), Development of Cenozoic basins in Thailand, *Mar. Pet. Geol.*, *8*, 84–97, doi:10.1016/0264-8172(91)90047-5.

Pongsapitch, W., S. Vedchakanchana, and P. Pongproyoon (1980), Petrology of the Pran Buri, Hua Hin metamorphic complex and geochemistry of gneiss in it, *Bull. Geol. Soc. Malays.*, *12*, 54–74.

Putthapiban, P. (1992), The Cretaceous-Tertiary granite magmatism in the west coast of peninsular Thailand and the Mergui Archipelago of Myanmar/Burma, paper presented at National Conference on Geological Resources of Thailand: Potential for Future Development, Dep. Min. Resour., Bangkok.

Putthapiban, P., and M. O. Schwartz (1994), Geochronology of the Southeast Asian tin belt granitoids, in *Metallogeny of Collisional Orogens*, edited by R. Seltmann, H. Kämpf and P. Möller, pp. 391–398, Czech Geol. Surv., Prague.

Rhodes, B. P., J. Blum, and T. Devine (2000), Structural development of the mid-Tertiary Doi Suthep metamorphic core complex and western Chiang Mai basin, northern Thailand, *J. Asian Earth Sci.*, *18*, 97–108, doi:10.1016/S1367-9120(99)00019-X.

Ridd, M. F. (1971), Faults in Southeast Asia, and the Andaman rhombochasm, *Nature*, *229*, 51–52.

Ridd, M. (2009), The Phuket Terrane: A Late Palaeozoic rift at the margin of Sibumasu, *J. Asian Earth Sci.*, *36*, 238–251, doi:10.1016/j.jseaes.2009.06.006.

Rodríguez, J., M. A. Cosca, J. I. G. Ibarguchi, and R. D. Dallmeyer (2003), Strain partitioning and preservation of $^{40}Ar/^{39}Ar$ ages during Variscan exhumation of a subducted crust (Malpica-Tui complex, NW Spain), *Lithos*, *70*, 111–139, doi:10.1016/S0024-4937(03)00095-1.

Rowley, D. B. (1998), Minimum age of initiation of collision between India and Asia north of Everest based on the subsidence history of the Zhepure mountain section, *J. Geol.*, *106*, 229–235, doi:10.1086/516018.

Schärer, U., L.-S. Zhang, and P. Tapponnier (1994), Duration of strike-slip movements in large shear zones: The Red River belt, China, *Earth Planet. Sci. Lett.*, *126*, 379–397, doi:10.1016/0012-821X(94)90119-8.

Searle, M. P. (2006), Role of the Red River Shear zone, Yunnan and Vietnam, in the continental extrusion of SE Asia, *J. Geol. Soc.*, *163*, 1025–1036, doi:10.1144/0016-76492005-144.

Searle, M. P. (2007), Reply to discussion on the role of the Red River Shear zone, Yunnan and Vietnam, in the continental extrusion of SE Asia, *J. Geol. Soc.*, *164*, 1253–1260.

Searle, M. P., and C. K. Morley (2011), Tectonic and thermal evolution of Thailand in the regional context of Southeast Asia, in *The Geology of Thailand*, edited by M. F. Ridd, A. J. Barber, and M. J. Crow, pp. 539–571, Geol. Soc., London.

Searle, M., R. I. Corfield, B. Stephenson, and J. Mccarron (1997), Structure of the North Indian continental margin in the Ladakh-Zanskar Himalayas: Implications for the timing of obduction of the Spontang ophiolite, India-Asia collision and deformation events in the Himalaya, *Geol. Mag.*, *134*, 297–316, doi:10.1017/S0016756897006857.

Searle, M. P., S. R. Noble, J. M. Cottle, D. J. Waters, A. H. G. Mitchell, T. Hlaing, and M. S. A. Horstwood (2007), Tectonic evolution of the Mogok metamorphic belt, Burma (Myanmar) constrained by U-Th-Pb dating of metamorphic and magmatic rocks, *Tectonics*, *26*, TC3014, doi:10.1029/2006TC002083.

Sevastjanova, I., B. Clements, R. Hall, E. A. Belousova, W. L. Griffin, and N. Pearson (2011), Granitic magmatism, basement ages, and provenance indicators in the Malay Peninsula: Insights from detrital zircon U-Pb and Hf-isotope data, *Gondwana Res.*, *19*, 1024–1039.

Silpalit, M., A. Meesook, S. Lovacharasupaphon, and P. Chaodumrong (1985), Changwat Prachuap Khiri Khan, in *Geological Map of Thailand*, 1:250,000, Dep. Min. Resour., Bangkok.

Simons, W. J. F., et al. (2007), A decade of GPS in Southeast Asia: Resolving Sundaland motion and boundaries, *J. Geophys. Res.*, *112*, B06420, doi:10.1029/2005JB003868.

Smith, J. B., M. E. Barley, D. I. Groves, B. Krapez, N. J. McNaughton, M. J. Bickle, and H. J. Chapman (1998), The Scholl shear zone, West Pilbara: Evidence for a terrane boundary structure from integrated tectonic analyses, SHRIMP U-Pb dating and isotopic and geochemical data of granitoids, *Precambrian Res.*, *88*, 143–171, doi:10.1016/S0301-9268(97)00067-3.

Sone, M., and I. Metcalfe (2008), Parallel Tethyan sutures in mainland Southeast Asia: New insights for Palaeo-Tethys closure and implications for the Indosinian Orogeny, *C. R. Geosci.*, *340*, 166–179, doi:10.1016/j.crte.2007.09.008.

Stauffer, P. H., and N. Mantajit (1981), Late Palaeozoic tilloids of Malaya, Thailand and Burma, in *Earth's Pre-Pleistocene Glacial Record*, edited by M. J. Hambrey and W. B. Harland, pp 331–337, Cambridge Univ. Press, Cambridge, U. K.

Steiger, R. H., and E. Jäger (1977), Subcommission on geochronology: Convention on the use of decay constants in geo- and cosmochronology, *Earth Planet. Sci. Lett.*, *36*, 359–362, doi:10.1016/0012-821X(77)90060-7.

Tapponnier, P., and P. Molnar (1977), Active faulting and tectonics in China, *J. Geophys. Res.*, *82*, 2905–2930, doi:10.1029/JB082i020p02905.

Tapponnier, P., G. Peltzer, A. Y. Le Dain, R. Armijo, and P. Cobbold (1982), Propagating extrusion tectonics in Asia: New insights from simple experiments with plasticine, *Geology*, *10*, 611–616, doi:10.1130/0091-7613(1982)10<611:PETIAN>2.0.CO;2.

Tapponnier, P., G. Peltzer, and R. Armijo (1986), On the mechanism of collision between India and Asia, in *Collision Tectonics*, edited by M. P. Coward and A. C. Ries, *Geol. Soc. Spec. Publ.*, 19, 115–157.

Tulyatid, J. (1991), Ar^{40}/Ar^{39} Geochronology study of deformed metagranitioid rocks adjacent to the Hua-Hin Pran Buri Fault System, Peninsular Thailand, Masters thesis, 151 pp., Queen's Univ., Kingston, Ont., Canada.

Ueno, K. (2003), The Permian fusulinoidean faunas of the Sibumasu and Baoshan blocks: Their implications for the palaeogeographic and paleoclimatologic reconstruction of the Cimmerian Continent, *Palaeogeogr. Palaeoclimatol. Palaeoecol.*, *193*, 1–24, doi:10.1016/S0031-0182(02)00708-3.

Upton, D. R. (1999), A regional fission track study of Thailand: Implications for thermal history and denudation, Ph.D. thesis, 417 pp., Univ. London, London.

Uttamo, W., C. F. Elders, and G. J. Nicols (2003), Relationships between Cenozoic strike-slip faulting and basin opening in northern Thailand, in *Intraplate Strike-Slip Deformation Belts*, edited by F. Storti et al., *Geol. Soc. Spec. Publ.*, 210, 89–108.

Vigny, C., A. Socquet, C. Rangin, N. Chamot-Rooke, M. Pubellier, M.-N. Bouin, G. Bertrand, and M. Becker (2003), Present-day crustal deformation around the Sagaing fault, Myanmar, *J. Geophys. Res.*, *108* (B11), 2533, doi:10.1029/2002JB001999.

Wang, E., B. C. Burchfiel, L. H. Royden, C. Liangzhong, C. Jishen, L. Wenxin, and C. Zhiliang (1998), Late Cenozoic Xianshuihe-Xiaojiang, Red River, and Dali fault systems of southwestern Sichuan and central Yunnan, China, *Spec. Pap. Geol. Soc. Am.*, *327*, 108 pp.

Wang, P. L., C. H. Lo, S. L. Chung, T. Y. Lee, C. Y. Lan, and T. van Thang (2000), Onset timing of left-lateral movement along the Ailao Shan-Red River Shear Zone: Ar-40/Ar-39 dating constraint from the Nam Dinh Area, northeastern Vietnam, *J. Asian Earth Sci.*, *18*, 281–292, doi:10.1016/S1367-9120(99)00064-4.

Watkinson, I. (2009), The kinematic history of the Khlong Marui and Ranong faults, Southern Thailand, Ph.D. thesis, 473 pp., Univ. London, London.

Watkinson, I., C. Elders, and R. Hall (2008), The kinematic history of the Khlong Marui and Ranong faults, southern Thailand, *J. Struct. Geol.*, *30*, 1554–1571, doi:10.1016/j.jsg.2008.09.001.

Yeh, M.-W., T.-Y. Lee, C.-H. Lo, S.-L. Chung, C.-Y. Lan, and T. T. Anh (2008), Structural evolution of the Day Nui Con Voi metamorphic complex: Implications on the development of the Red River Shear Zone, northern Vietnam, *J. Struct. Geol.*, *30*, 1540–1553, doi:10.1016/j.jsg.2008.08.007.

Zhang, L. S., and U. Schärer (1999), Age and origin of magmatism along the Cenozoic Red River shear belt, China, *Contrib. Mineral. Petrol.*, *134*, 67–85, doi:10.1007/s004100050469.

Zhu, B., W. S. F. Kidd, D. B. Rowley, B. S. Currie, and N. Shafique (2005), Age of initiation of the India-Asia collision in the east-central Himalaya, *J. Geol.*, *113*, 265–285, doi:10.1086/428805.

G. Batt, Centre for Exploration Targeting, John de Laeter Centre for Mass Spectrometry, University of Western Australia, Perth, WA 6009, Australia.

C. Elders, R. Hall, and I. Watkinson, SE Asia Research Group, Department of Earth Sciences, Royal Holloway, University of London, TW20 0EX, UK. (i.watkinson@es.rhul.ac.uk)

F. Jourdan, Western Australian Argon Isotope Facility, Department of Applied Geology and John de Laeter Centre for Mass Spectrometry, Curtin University, Perth, WA 6845, Australia.

N. J. McNaughton, Department of Imaging and Applied Physics, John de Laeter Centre for Mass Spectrometry, Curtin University, Perth, WA 6845, Australia.